NASA CONTRACTOR REPORT

A STUDY OF CHARGE STORAGE IN SILICON OXIDE RESULTING FROM NON-PENETRATING ELECTRON IRRADIATION

by M. Simons, L. K. Monteith, and J. R. Hauser

Prepared by
RESEARCH TRIANGLE INSTITUTE
Research Triangle Park, N. C.
for Langley Research Center

NATIONAL AERONAUTICS AND SPACE ADMINISTRATION • WASHINGTON, D. C. • JUNE 1968

NASA CR-1088

A STUDY OF CHARGE STORAGE IN SILICON OXIDE RESULTING FROM NON-PENETRATING ELECTRON IRRADIATION

By M. Simons, L. K. Monteith,
and J. R. Hauser

Prepared under Contract No. NAS 1-6900 by
RESEARCH TRIANGLE INSTITUTE
Research Triangle Park, N.C.

for Langley Research Center

NATIONAL AERONAUTICS AND SPACE ADMINISTRATION

For sale by the Clearinghouse for Federal Scientific and Technical Information
Springfield, Virginia 22151 – CFSTI price $3.00

ABSTRACT

Charge storage in silicon dioxide resulting from low energy electron irradiation has been observed. The positive charge build-up has been studied in MOS type structures for various oxide thicknesses as a function of beam energy, electron fluence, sample bias, electrode thickness, and a number of oxide-related parameters. The effective radiation-induced oxide charge appears to be a function of beam energy dissipated within the oxide near the oxide-silicon interface; this charge increases with electron fluence up to a saturation level which was observed in some steam-grown oxides; the experimentally observed dependence of induced charge on applied bias is compared with that predicted by several models for charge accumulation.

Optical and thermal annealing of the trapped charge has been studied in an effort to derive information on the nature of the oxide trapping levels. Reduction of trapped charge by irradiation at small negative biases has also been explored.

Finally the development of a two-carrier model for space charge build-up in an MOS structure is discussed and the experimental results obtained for silicon dioxide are related to device performance in the radiation environment.

CONTENTS

LIST OF ILLUSTRATIONS

LIST OF ILLUSTRATIONS (continued)

A STUDY OF CHARGE STORAGE IN SILICON OXIDE RESULTING FROM NON-PENETRATING ELECTRON IRRADIATION

By M. Simons, L. K. Monteith, and J. R. Hauser*

SECTION I

INTRODUCTION

Thermally grown layers of silicon dioxide are widely used for passivation of present day integrated circuits and silicon devices. Not only are SiO_2 layers ideal for terminating the silicon lattice in such a way as to minimize surface state densities, but they also serve as convenient insulating surfaces on which to deposit intraconnecting paths and passive components. In metal-oxide-silicon (MOS) devices where the oxide serves as an integral part of the active device, oxide properties are of fundamental importance. For example, MOS device characteristics can be altered to the point of failure by extraneous charge in the oxide.

One such method by which space charge is introduced into silicon dioxide is through exposure to ionizing radiation. Space charge induced in SiO_2 in this manner can severely limit the performance of both junction and MOS type devices employed in a radiation environment. It is the purpose of this work to obtain a better understanding of the radiation-induced space charge build-up in silicon dioxide through the use of non-penetrating electron radiation, which allows isolation of the oxide effects from interface and substrate effects in an MOS structure. In addition, charge release will be studied to gain some insight into the nature of this trapped oxide charge.

Because of their extreme sensitivity to the various oxide properties, MOS structures become an invaluable tool in the study of such properties. The capacitance, conductance, and bias characteristics of the MOS device can be utilized to obtain information on mobile and fixed charge in the oxide as well as on states present at the interface. The capacitance versus bias (C-V) characteristics of the MOS structure are particularly useful in measuring radiation-induced oxide charge and were utilized extensively during this work. Before proceeding to a discussion of the experimental work, the MOS structure and its associated C-V characteristics will be briefly reviewed.

The silicon surface layer of the MOS configuration can be in one of three states depending upon the applied potential. These are accumulation, depletion, and inversion. Figure 1 illustrates the energy bands and charge

---

* Assistant Professor of Electrical Engineering, North Carolina State University, Raleigh, N. C. (Consultant at Research Triangle Institute).

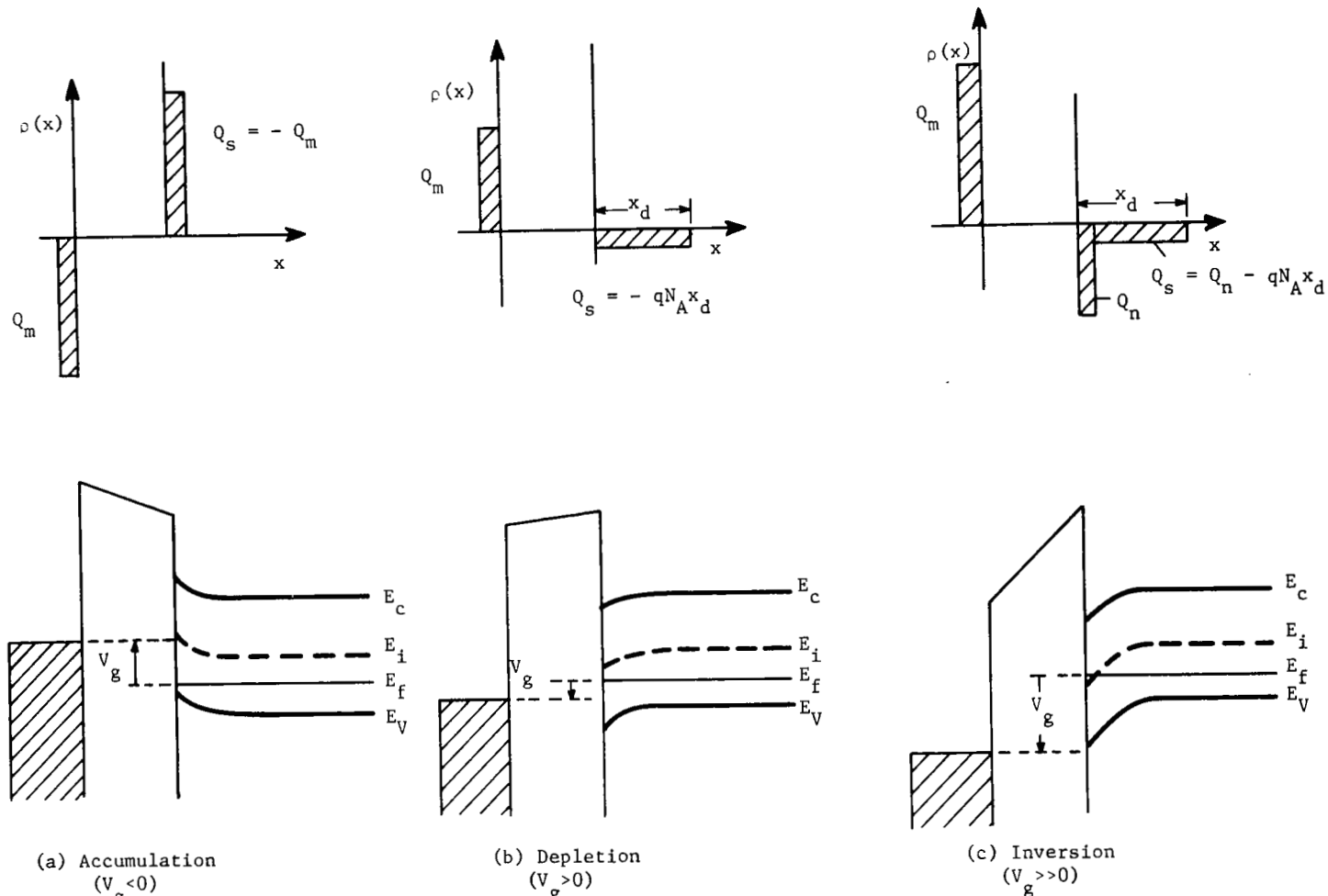

(a) Accumulation (V_g<0)

(b) Depletion (V_g>0)

(c) Inversion (V_g>>0)

Figure 1. Charge Distribution (above) and Band Structure (below) for P-Type MOS Structure in Each of Three Bias Regimes

distributions for each of these three cases for an ideal structure (no oxide charge) utilizing a p-type substrate. When the metal electrode is biased negatively the holes or majority carriers are attracted toward the interface causing this region to become more p-type or "accumulated" as indicated in Fig. 1(a). The capacitance per unit area of the system is simply that due to the oxide and is expressed by

$$C = C_o = \frac{\varepsilon_{ox}}{x_o} . \qquad (1)$$

For small positive biases majority carriers are repelled from the interface leaving the ionized acceptor impurity ions to form a negative space charge or depletion region as shown in Fig. 1(b). As the depletion region widens with increasing bias, the overall capacitance decreases from C_o and becomes essentially the series combination of the depletion region and oxide capacitances. Upon further increase of the applied positive bias, the silicon surface begins to invert and the depletion width saturates. This condition is shown in Fig. 1(c). Here, depending on the frequency of the applied signal, the MOS capacitance can either rise toward C_o or remain at the lower level determined by the series combination of the two capacitances. At frequencies sufficiently low for the minority carriers in the inversion layer to equilibrate or follow the applied signal, the capacitance will return to C_o as the bias is increased further. At higher frequencies only the majority carriers can follow the applied signal so the capacitance remains at the lower level. Figure 2 illustrates ideal high and low frequency C-V characteristics and the three regimes just described. The same argument applies in the case of an n-type substrate except that the voltage polarities are reversed. A number of good theoretical treatments of the MOS structure have been published (Refs. 1 - 5), so this theory will not be repeated here. Ideal curves for MOS capacity and surface potential have been computed by Goetzberger (Ref. 4) for various oxide thicknesses and substrate resistivities. These curves are useful in comparing with the measured characteristics.

Any positive charge trapped in the oxide of an MOS structure will induce a negative charge in the underlying silicon surface. This has the effect of producing a parallel displacement of the C-V characteristics toward a more negative voltage. This voltage displacement ΔV is, of course, a function of the image charge induced at the silicon surface. If N_{ss} is the effective density of surface charges reflected at the oxide-silicon interface, then

$$N_{ss} = \frac{C_o \, \Delta V}{q} = \frac{\varepsilon_{ox} \, \Delta V}{1.6 \times 10^{-19} \, x_o} , \qquad (2)$$

where ε_{ox} and x_o are the MKS oxide dielectric constant and thickness, respectively.

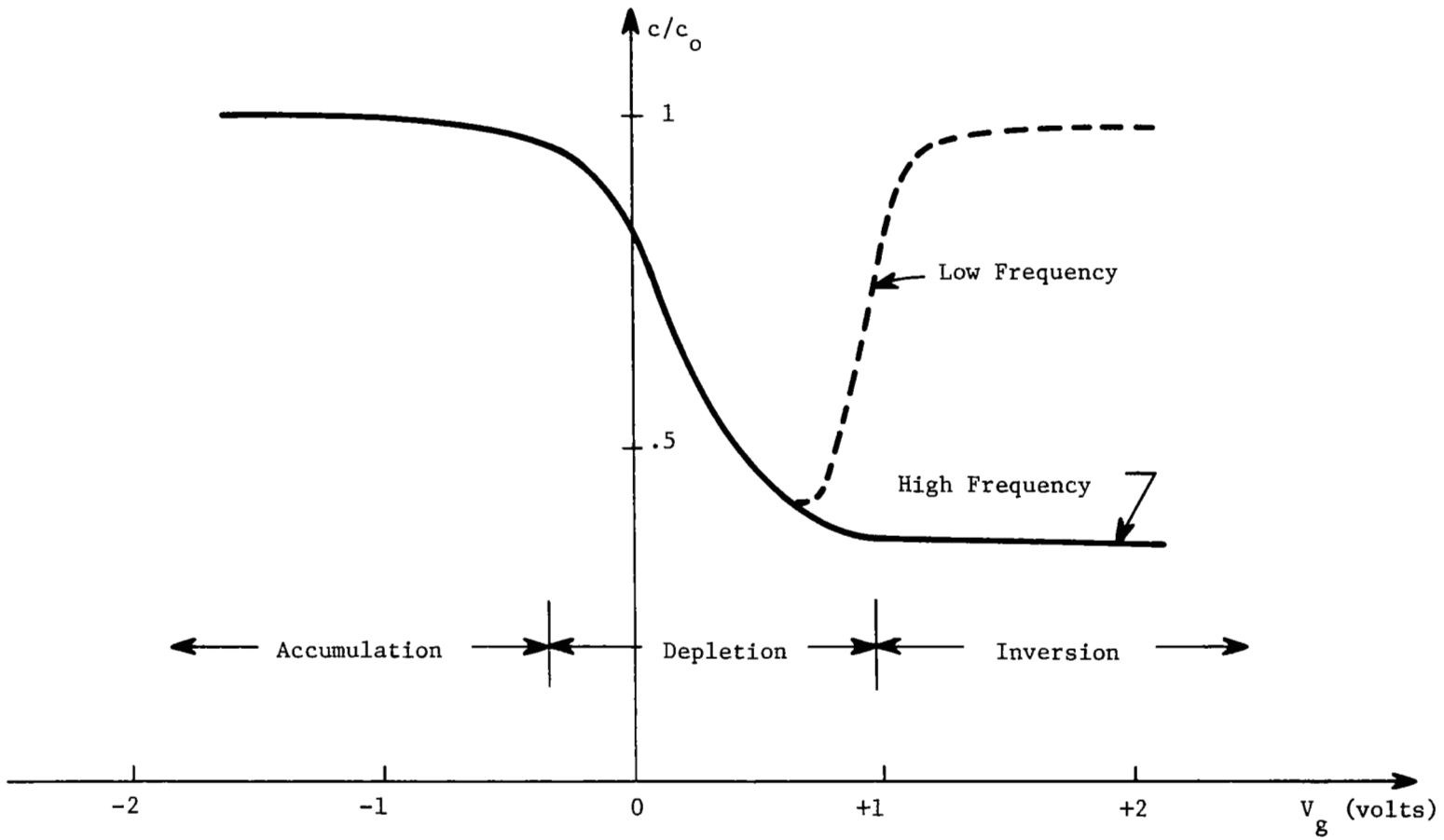

Figure 2. Ideal C-V Characteristic for P-Type MOS Structure

Physically realizable MOS structures are somewhat less than ideal in that the oxide contains a finite positive charge both in interface states and in the bulk. Thus, the initial C-V characteristic is displaced toward a negative voltage; also, since any charge residing in fast interface states is a function of the position the Fermi level at the interface, the presence of these states alters the manner in which the surface potential varies with bias. This causes some deterioration of the slope of the C-V characteristic in the depletion region (Ref. 5).

The fabrication steps required in preparing an MOS structure and the techniques used in making C-V measurements during this work are described in the following section.

SECTION II

EXPERIMENTAL PROCEDURE

Preparation and Characterization of MOS Samples

Considerable care is required in the preparation of MOS type devices to minimize extraneous oxide charge resulting from both impurity ions in the oxide and surface states at the oxide-silicon interface. Since one of the objectives of this research was to investigate the role of ionic contamination in radiation-induced charge build-up in SiO_2, a major effort was directed toward reducing these extraneous charge sources to an absolute minimum level.

Although much research has recently been carried out on the metal-oxide-silicon system, particularly by research groups associated with device manufacturers, there has been a real reluctance to reveal processing details involved in the preparation of high quality oxides. The usual advice given is simply to clean up the wafer cleaning and oxidation procedures. Consequently, a variety of different wafer cleaning procedures, oxidation methods, post-oxidation treatments, and metallization techniques had to be tried and evaluated in an effort to find an optimum process for sample preparation. Although the procedure selected is not quite state-of-the-art, the results obtained were sufficiently good to warrant a description of the oxidation equipment and the steps followed in preparing the samples.

A diagram of the thermal oxidation system is shown in Fig. 3. A Lindberg/Heavy Duty high temperature laboratory furnace, employing silicon carbide heating elements capable of operation up to 1482°C, furnished the regulated temperature necessary for oxidation. Temperature regulation was provided by a built-in control unit employing a platinum-platinum rhodium thermocouple. A double-walled quartz oxidation tube was designed to allow the flow of an inert gas down the tube between inner and outer walls for the purpose of sweeping out sodium or other impurity ions which might diffuse from the furnace through the quartz and contaminate the samples. Silicon oxidations were carried out by passing either oxygen or steam through the center tube where the samples were mounted on a slotted quartz boat. Nitrogen was directed through the center tube during annealing cycles or when the system was not in use. Commercial high purity bottled gases passed through one-half micron filters served as the oxygen and nitrogen sources. Steam was generated by boiling 16-18 megohm-cm, deionized water in a quartz flask. All quartz-ware was etched with HF and rinsed with deionized water before use.

The oxides studied in this work were grown on boron-doped single crystal silicon wafers of both 10 and 100 ohm-cm resistivity. The wafers, which were obtained from Monsanto Chemical Company, had a (111) surface

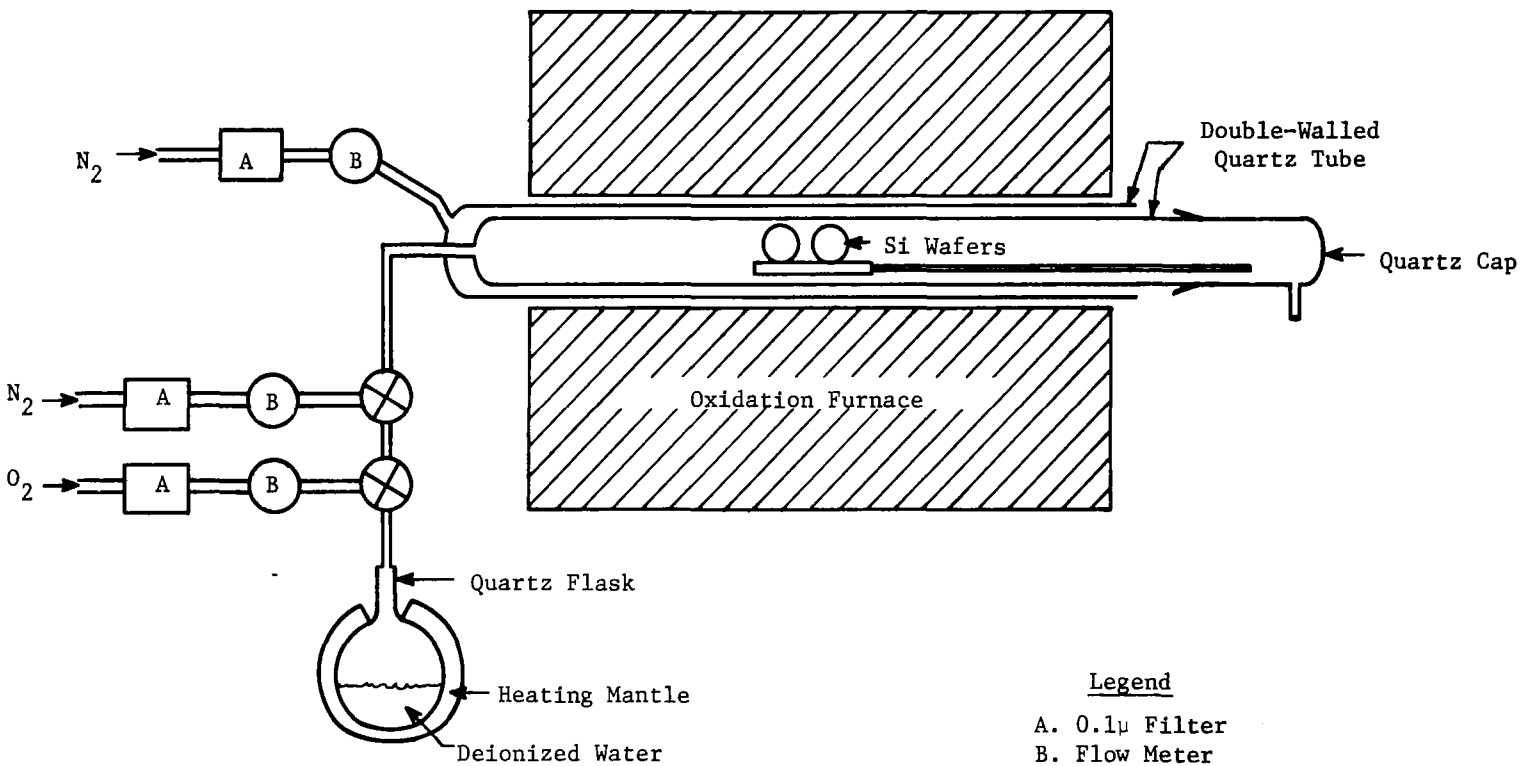

Figure 3. Thermal Oxidation System

orientation and were chemically polished by the manufacturer. It has been established that the pre-oxidation wafer cleaning technique is very critical in order to maintain a minimum level of surface contamination, which, of course, is essential for the formation of high quality oxides. The following cleaning technique yielded the best results during this work. First, the wafers were boiled for several minutes in trichloroethylene (TCE) and then ultrasonically cleaned in the same solvent for 2 minutes. These steps were repeated using acetone as a solvent. After a 2 to 5 minute rinse in deionized water, the wafers were heated in concentrated nitric acid for 10-15 minutes. A second rinse in deionized water was followed by a one minute soak in a 48% HF solution. After a final 5 to 10 minute rinse in deionized water, the wafers were dried in a jet of dry nitrogen and immediately loaded onto the quartz boat which was inserted into the furnace.

All oxides were grown at either 1000°C or 1100°C. The kinetics of silicon oxidation in both steam and dry O_2 is well understood and has been discussed in some detail (Ref. 6). Oxide thickness could be controlled to within 5 or 10% by careful control of oxidation time and temperature. The color of the oxides when viewed perpendicularly was found to be a convenient means of checking the thickness to within several hundred angstroms (Ref. 6). After the desired oxidation time had elapsed, the wafers were annealed from 20-30 minutes in nitrogen at the oxidation temperature, then rapidly withdrawn to the end of the tube where they were allowed to cool to room temperature. This anneal treatment and subsequent rapid removal from the furnace hot zone has been reported to minimize that surface state charge at the oxide-silicon interface which arises because of excess silicon species introduced into the oxide layer near the silicon during oxidation (Ref. 7).

Following removal of the wafers from the furnace, the front surface of each wafer was waxed to a glass slide with apiezon wax and the oxide removed from the rear surface with HF. The protective wax was then removed from the wafer by boiling several times in TCE and acetone followed by a deionized water rinse. Next, from 10 to 20 percent of the oxide on the front surface was removed using a standard etchant consisting of a dilute HF solution buffered with amonium fluoride. Etching away the outer oxide layer serves to remove contaminants introduced by the apiezon wax. Also, since neutron activation analysis of oxidized silicon has shown that sodium ions, presumably introduced during oxidation, tend to congregate at the outer oxide surface (Ref. 8), removal of the outer oxide layer helps reduce this source of contamination. After a final five-minute rinse in deionized water the wafers were dried in nitrogen and immediately loaded into a vacuum chamber for evaporation of metal electrodes and ohmic contacts.

A single electrode, generally about one centimeter in diameter with a 1 to 2 mm wide stripe extending radially outward for contact to the sample holder, was evaporated through a metal mask onto each wafer when the chamber pressure reached 2×10^{-5} to 5×10^{-5} torr. Most samples were equipped with aluminum electrodes evaporated to various thicknesses from high purity aluminum

on a tungsten filament; several samples bearing gold and silver electrodes were also prepared. A shutter located between the filament and wafers was employed during all evaporations to shield the samples from impurity atoms emitted during filament bakeout prior to metallization. Deposition of an aluminum ohmic contact on the rear surface of each wafer completed preparation of the samples. Samples awaiting irradiation were stored at room temperature in a glass container filled with nitrogen.

Characterization of the MOS samples was accomplished primarily by C-V plots although dissipation factor and dc resistance were also checked. C-V measurements indicated that oxides grown in dry oxygen were generally more stable and had a lower initial oxide charge than those grown in steam. Usually this initial or fixed positive charge in both type oxides could be reduced further by annealing the completed samples at 300°C for about 5 minutes in a nitrogen environment. This charge reduction probably results from the thermal release of trapped charge from states at the oxide-silicon interface and perhaps also from the tendency of ionic impurities to diffuse away from this interface. Annealed oxygen-grown oxides were were prepared having fixed surface densities (N_{ss}) down to 2×10^{11} cm^{-2}.

In addition to the fixed oxide charge, alkali ions constitute a mobile charge source at elevated temperatures and drift in the presence of an applied electric field. The presence of sodium in the best available quartz, as well as in apparatus used in processing silicon, practically insures the presence of this element in thermally grown silicon oxides. A second major source of alkali contamination of MOS devices is generally thought to be the evaporants and filaments used during electrode deposition. The combination of aluminum evaporated from a tungsten filament has been reported to be a particularly dirty combination (Ref. 9). However, during this work no significant differences were noted in mobile charge densities between samples with electrodes of aluminum, gold, or silver evaporated from tungsten filaments and aluminum deposited by electron beam evaporation. For 2700 Å oxides, typical flat band voltage shifts of 7 volts were experienced after a 5 minute temperature-bias treatment at 300°C and 5×10^5 V/cm. This voltage shift is equivalent to approximately 5×10^{11} mobile charges per cm^2. This shift was reduced to 2 volts or about 2×10^{11} mobile charges per cm^2 for a 2500 Å sample whose oxide had been exposed to a brief phosphorus diffusion cycle immediately after oxidation. A 5000 Å phosphorus-treated sample was prepared with a mobile charge density of 9×10^{10} cm^{-2}. Radioactive tracer experiments have shown that surface passivation layers of P_2O_5 glass on silicon dioxide act as a getter or trap for sodium ions and prevent their drift into the oxide (Ref. 10).

Figure 4 shows a block diagram of the C-V plotting system used to obtain initial oxide charge data as well as that following irradiation. The ac voltage across resistor R (where $R << X_C$) is proportional to the unknown

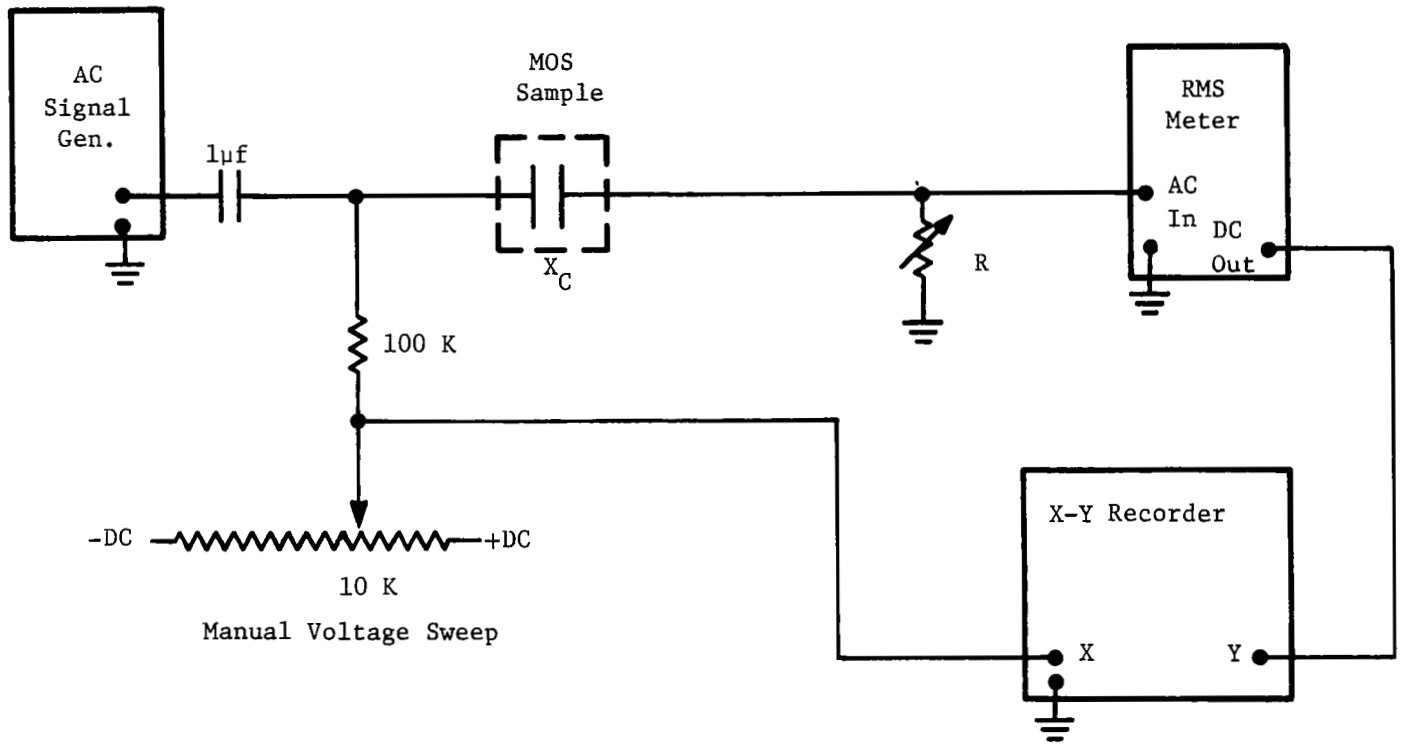

Figure 4. Capacitance vs. Voltage Plotting System

capacitance. The RMS voltmeter provides a dc output to drive the y-axis of the x-y recorder. A manual voltage sweep was found convenient so that the sweep rate could be retarded in the depletion voltage region where the capacitance dip occurs and increased elsewhere, thereby speeding up the overall operation. The C-V plot was independent of the sweep rate provided the rate did not exceed the system response time. C-V measurements were normally made at a signal frequency of 100 kHz. Typical 100 kc C-V characteristics made before and after exposure to electron radiation are shown in Fig. 5. The effective density of positive charge introduced into the oxide is determined from ΔV using Eq. (2). The slope of the irradiated characteristic in the depletion region was frequently observed to diminish with increasing exposure. This could result either from the introduction of fast interface states by the incident radiation or from a nonuniformity in electron exposure over the area beneath the sample electrode.

Several MOS samples with evaporated silicon monoxide as a dielectric were prepared for comparison with thermally grown SiO_2 films. The SiO was evaporated to thicknesses up to 3.5 microns from an R. D. Mathis Co.* oven onto properly cleaned p-type silicon substrates. An aluminum electrode evaporated over the oxide completed the MOS structure. Samples with oxides less than about 2 microns thick were unsatisfactory because of low oxide

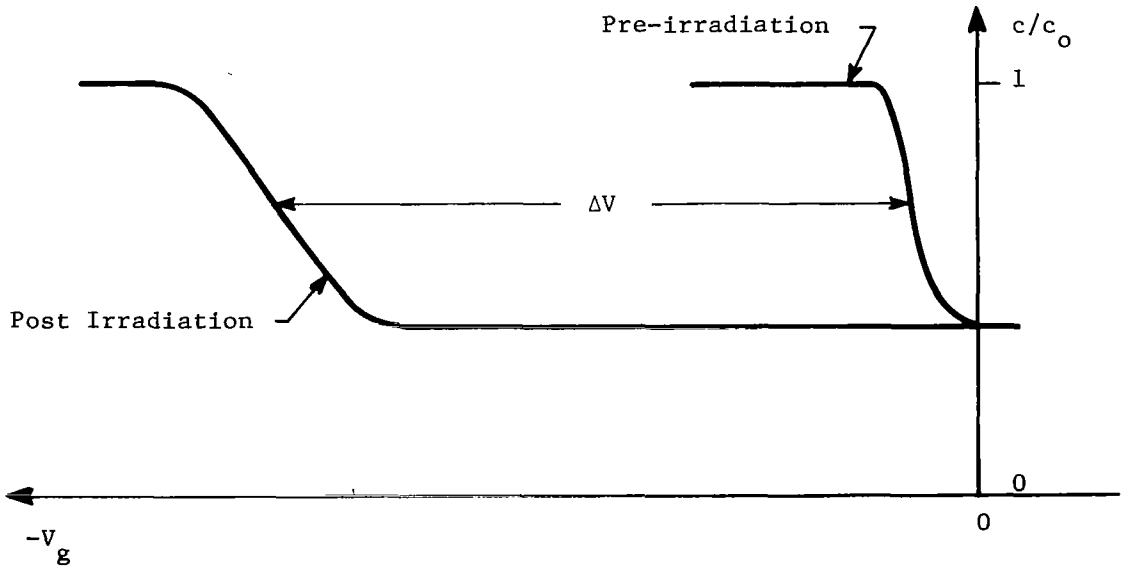

Figure 5. Radiation Induced Shift in MOS C-V Characteristic

* 1345 Gaylord St., Long Beach, Calif. 90813.

resistivity. Attempts to make C-V plots on the SiO structures were unsuccessful either because of the low oxide resistance or due to its excessive thickness. The thickness of SiO films was measured using standard optical interferometer techniques. Since C-V plots could not be used to measure the radiation-induced charge build-up and release in the SiO samples, external charge release measurements were made in these units. These measurements simply involve observation of the charge transfer in an external circuit following irradiation. Frequently the distribution of oxide charge is inferred from this type data. A complete discussion of these techniques is contained in Refs. 11 and 12.

Electron Irradiations

Most of the electron irradiations conducted during the project were of relatively low energy (less than 30 keV), since the primary objective of the contract was to study the effects produced by non-penetrating electrons. A Brad-Thompson Model 776-W electron gun served as the low energy electron source. The electrons are emitted from a hot tungsten filament and accelerated through a dc potential regulated to within $\pm$ 2%. The electron beam was sufficiently defocused to provide a uniform flux density over a target area of approximately 1 cm^2. The beam current density could be accurately controlled from 10^{-10} amps/cm^2 up to about 10^{-5} amps/cm^2. Electrostatic and magnetic focusing together with an electrostatic deflection system are contained in the cylindrical gun housing. The gun was mounted on one side of a 12 inch cubic irradiation chamber fabricated from 3/4 inch aluminum to provide operator protection and electrostatic shielding. Chamber pressures were maintained at 10^{-5} torr or below during all irradiations by an oil diffusion pump attached to the bottom port of the aluminum chamber.

The experimental arrangement inside the chamber is shown in Fig. 6. The silicon wafer containing the MOS structure was spring-clipped into a recessed area of a 1/2 inch aluminum sample holder with the sample electrode centered over a beam aperture. The aluminum holder in turn was attached to the bottom of a one-foot section of stainless steel tubing extending through a vacuum feedthrough in the top of the chamber. The tube could be filled with liquid nitrogen to reduce the sample temperature. Electrical contact to the sample was maintained through the spring clip to the silicon ohmic contact and through the aluminum holder to the irradiated electrode. The spring clip was insulated from the holder by a ceramic stand-off recessed into the aluminum to reduce charge accumulation on the insulator surface. A shutter containing an aluminum pick-up button was used in positioning the beam, measuring beam current, and controlling sample exposure intervals. An aluminum plate with a circular aperture was positioned between the shutter and electron gun to help collimate the beam. Observation and additional access were made possible by a stainless steel plate containing a quartz observation window on one side of the chamber.

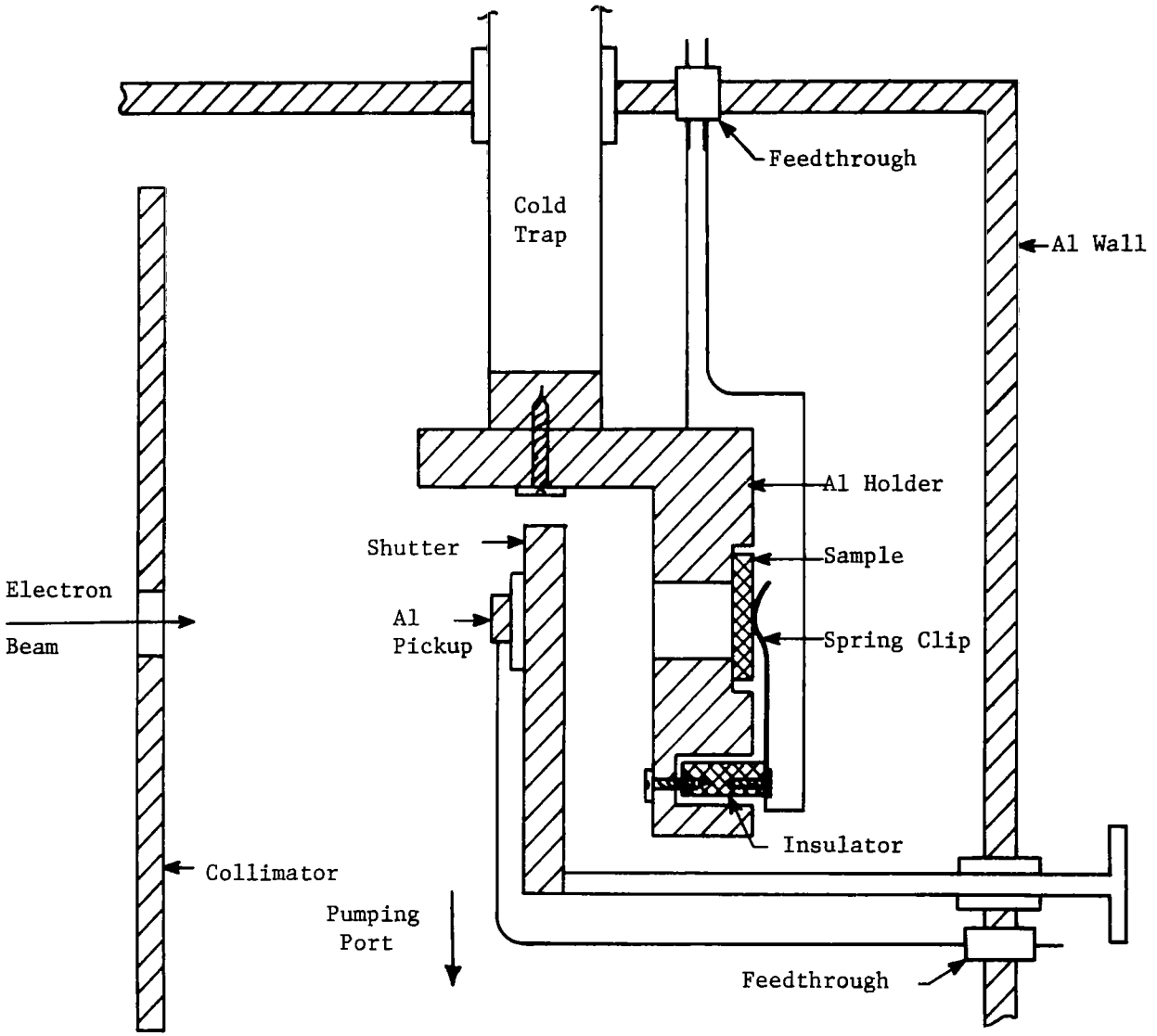

Figure 6. Irradiation Chamber

Since the backscattering coefficient and secondary electron yield for bulk aluminum are both significant, a correction factor had to be used in finding the primary beam current from the current measured at the aluminum pick-up. The backscattering coefficient for bulk aluminum has been reported at 0.14 over the energy range of interest, while the secondary yield varies from 0.2 at 20 keV up to about 0.7 at 2 or 3 keV (Ref. 13). It is estimated that the corrected primary beam currents could have been in error by 25% at the lower energies.

The charge build-up in the oxide of an irradiated MOS sample was measured following each exposure increment. The induced charge build-up was obtained as a function of electron fluence with beam energy and sample bias as parameters. Since the exposure rate was found to have at most only a second order effect on the charge build-up, either the beam current or the exposure time could be varied during a given sequence to increase the exposure increment. An irradiation sequence was terminated whenever the total induced charge in the oxide became sufficiently large that measurement of this charge required the application of an electric field approaching dielectric breakdown of the oxide. For SiO_2 prepared in dry oxygen, breakdown occurred in the neighborhood of 2×10^6 volts per cm. Steam oxides usually required a higher field to produce breakdown.

Irradiations were conducted from 3 keV up to 30 keV at fluences in the range between 10^{10} and 10^{14} e/cm^2. Beam currents were varied between 10^{-10} and 10^{-8} $amps/cm^2$, which is equivalent to flux densities from 6.2×10^8 to 6.2×10^{10} electrons per cm^2 per sec.

A series of high energy irradiations were carried out using the 1 MeV Dynamitron accelerator at Langley Research Center in order to obtain additional information in the charge build-up in SiO_2 as a function of electron energy. In this accelerator the swept electron beam covered sufficient area so that four MOS samples could be exposed simultaneously. The samples were mounted along the center line of a rectangular aluminum holder in much the same manner as described for low energy irradiations. The beam current, which was measured by a Faraday cup located between the samples, was averaged over the isoceles trangular sweep cycle of approximately 85 ms duration. Irradiations were performed at average flux densities of 10^9 and 10^{10} electrons per cm^2 per sec. During test runs made prior to the 200 keV and 1 MeV sample irradiations, cobalt glass dosimeters indicated beam uniformity over the target area to be within $\pm$ 10% of that measured at the Faraday cup. Again, C-V measurements were made on each unit following selected exposure increments until the desired total exposure was reached.

SECTION III

CHARGE BUILD-UP

General

Exposure of silicon MOS type structures to ionizing radiation is consistently reported to produce a positive charge build-up in the oxide regardless of the type of irradiation. The positive charge in the oxide induces a negative charge in the silicon and results in a parallel shift of the C-V characteristic in the negative direction along the voltage axis. Although the C-V displacement is a convenient means for studying the charge build-up process in silicon dioxide, a corresponding shift in the I-V characteristics of MOS type transistors unfortunately serves to degrade the performance of these devices in a radiation environment. It has generally been observed that such factors as the electric field in the oxide, type and energy of irradiation, and method of oxidation have a strong effect on the induced charge. Other factors such as flux density, temperature, and various oxide characteristics have been found to play a lesser role in the build-up process.

A major goal of this work was to study the charge accumulation process in electron-irradiated SiO_2. To accomplish this goal, irradiations were conducted on different type oxides as a function of sample bias, oxide thickness, electron energy, and electron fluence. Variation of the electron energy from levels as low as 3 keV allowed the induced charge to be studied as a function of the beam penetration depth in the oxide. Irradiations were also conducted on samples having different types and thicknesses of metal electrodes to see how variation of these parameters would affect the induced charge.

Most of the oxides irradiated were prepared in oxygen rather than steam since steam-grown oxides usually had a higher level of residual contamination and were less stable under temperature-bias stress. Since no information was available as to the role which sodium and other oxide contaminants play in the charge build-up process, oxides with minimum impurity concentrations were investigated before proceeding to the contaminated oxides. Several samples with steam-grown oxides were prepared and irradiated to provide a comparison with the charge accumulation observed in oxygen oxides.

The general procedure followed in carrying out the irradiations was to expose a sample under a given set of conditions and measure the C-V displacement after selected exposure increments over several orders of magnitude of electron fluence. The effective oxide charge was then removed or reduced either by thermal annealing or by irradiation at a small negative bias as described in the next section. The same sample could then be re-irradiated under a different set of conditions, thereby preventing variations which might arise from using a different sample. Reproducibility

of data on a given sample was good and usually the variations between different samples having oxides grown simultaneously were relatively small.

Effect of Sample Bias

In order for a net charge density to be induced in a dielectric, separation and selective trapping of charged carriers are required. Thus, the electric field present in silicon dioxide during irradiation would be expected to have an effect on the distribution of trapped charge by influencing the motion and distribution of radiation induced free carriers. Figure 7 shows ΔV for the C-V characteristic as a function of 5 keV electron fluence for several values of positive bias applied to a sample having a 2500 Å oxygen-grown oxide. The negative voltage displacement or induced charge increases rapidly with the total exposure and shows a strong dependence on the bias applied during irradiation. No sign of saturation is exhibited by the displacement curves which extend to a maximum ΔV of 50 volts, where irradiations were terminated to prevent the field applied during C-V measurement (approximately 2×10^6 V/cm) from producing localized shorts in the oxide. If it is assumed that most of the positive charge is trapped close to the oxide-silicon interface, then 50 volts corresponds to an induced charge density of 4×10^{12} cm^{-2}.

The same data for a sample having a 2500 Å oxide grown in steam is shown in Fig. 8. Again the induced positive charge is strongly dependent on applied bias, although the steam oxide exhibits a much lower radiation sensitivity than the oxygen oxide, particularly after undergoing a 300°C anneal for several minutes. Another significant difference is the saturation of ΔV in the annealed steam oxide. This occurs in the fluence range above 10^{12} - 10^{13} e/cm^2, particularly at lower levels of applied bias. With the exception of the oxidation method, identical processing steps were followed in preparing the two samples and, in this case, both samples exhibited almost the same level of oxide contamination. The marked difference in radiation sensitivities between the two oxides indicated that the steam oxide has a significantly lower trap density.

Figure 9 illustrates ΔV as a function of the positive and negative bias applied during irradiation for both 2500 Å oxide samples. The voltage displacement plotted for the steam sample corresponds approximately to the saturation value (ΔV_{sat}), particularly for lower biases. While ΔV has just about saturated at 5×10^{12} e/cm^2 in the steam oxide, a fluence of only 1.5×10^{11} e/cm^2 is seen to produce a comparable voltage displacement in the non-saturating oxygen oxide at a given positive bias. It is interesting to note that although the curve plotted for the oxygen sample does not

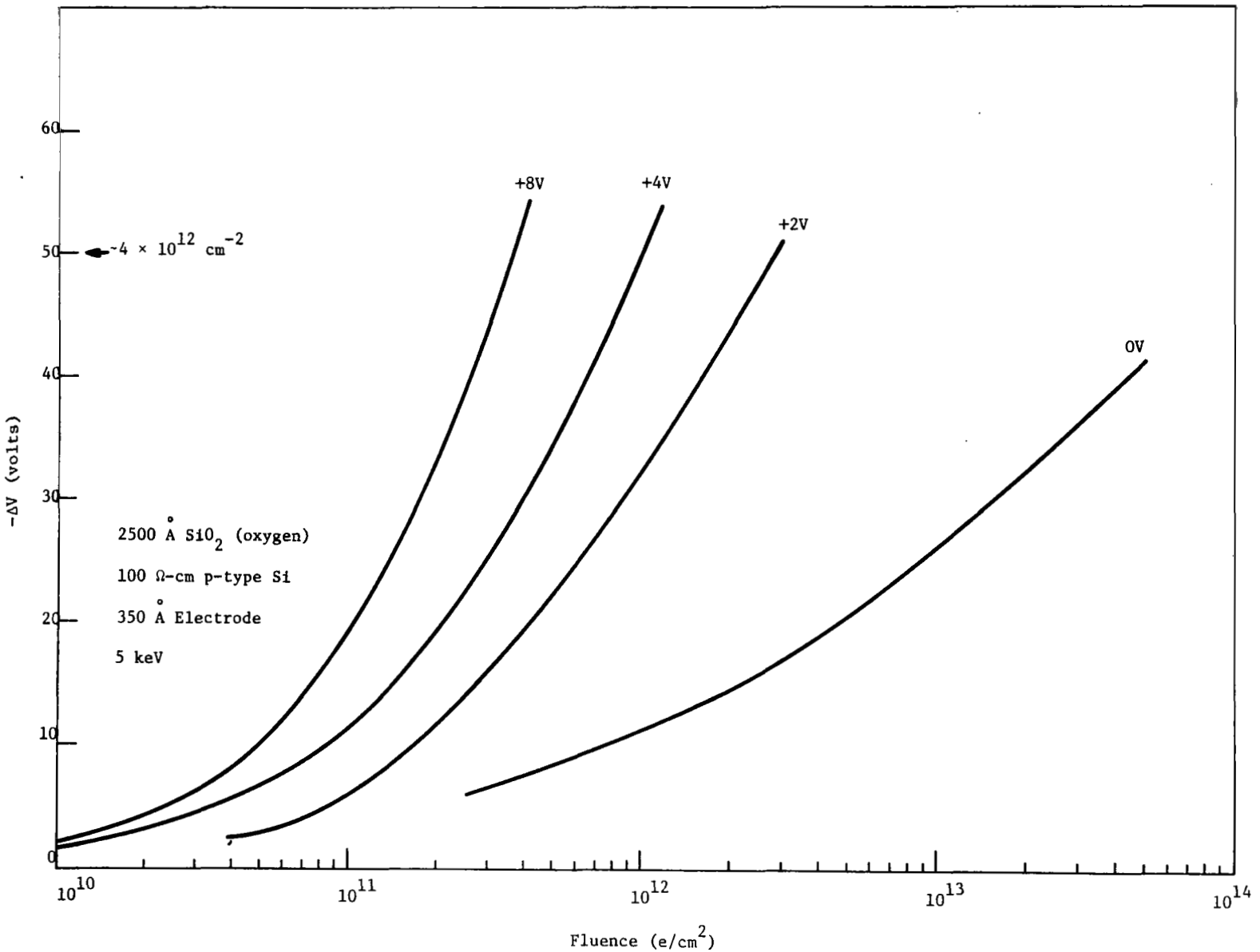

Figure 7. Charge Build-up vs. Fluence in 2500 Å Oxygen Oxide at Various Positive Bias Levels

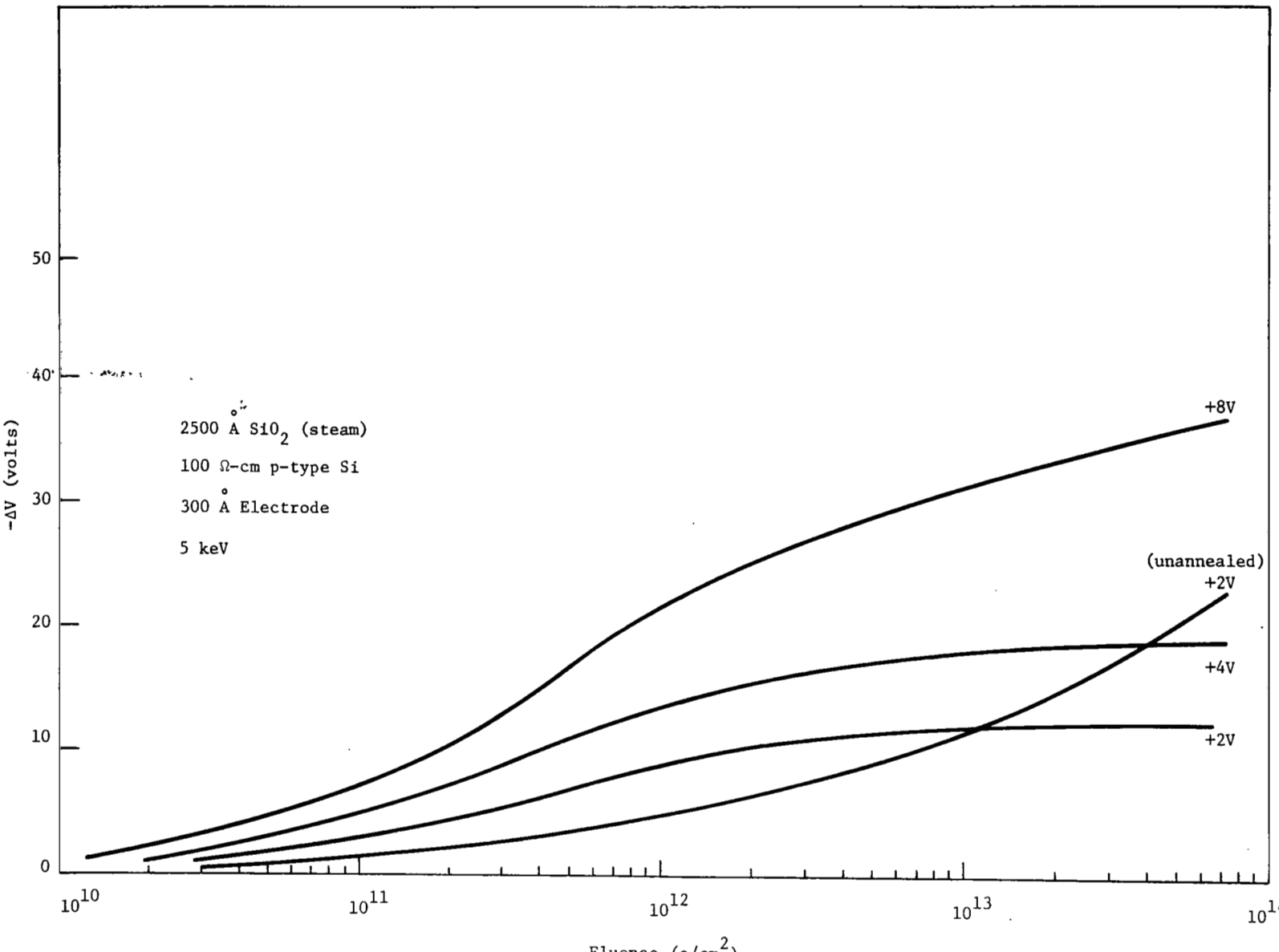

Figure 8. Charge Build-up vs. Fluence in 2500 Å Steam Oxide at Various Positive Bias Levels

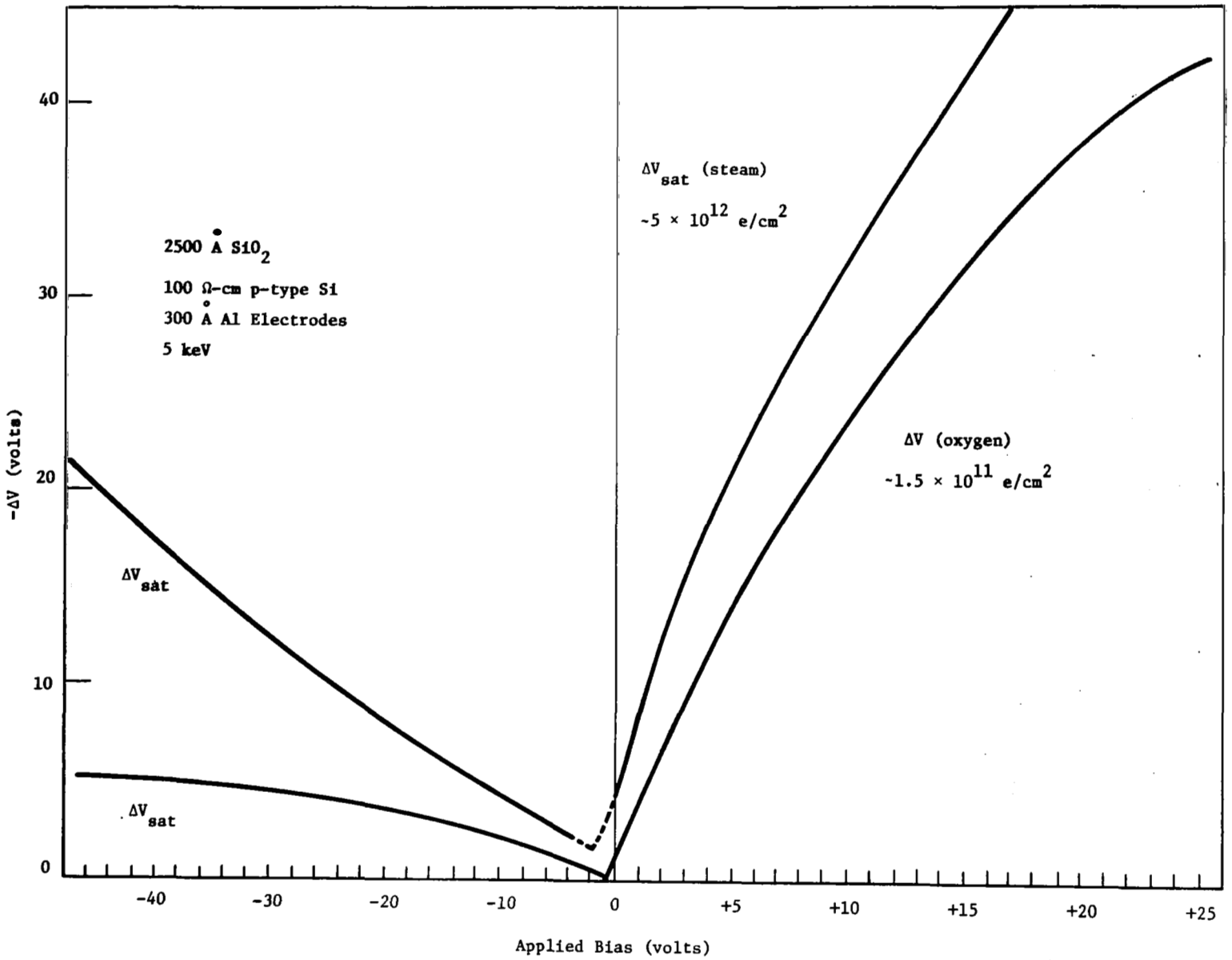

Figure 9. Charge Build-up vs. Applied Bias in 2500 Å Oxides

represent the saturation displacement, both curves exhibit a similar functional dependence on positive bias. At small biases ΔV varies almost linearly with applied bias; as the bias increases ΔV falls off from a linear toward a parabolic dependence. At negative biases ΔV_{sat} is smaller in the oxygen oxide and tends to level off or saturate as the applied bias is increased in the negative direction. In both units minimum ΔV occurs at a small negative bias, somewhere in the vicinity of -1 volt. It is at this bias that many samples can be irradiated at a suitable energy to return the C-V plot to its initial pre-irradiation position (see Sec. IV).

The linearity of charge build-up with applied positive bias is emphasized in Fig. 10, which shows ΔV as a function of positive and negative biases for a 9200 Å oxygen oxide irradiated with 14 keV electrons at a fluence of approximately 10^{11} e/cm^2. In this case ΔV, which does not represent the saturation displacement, shows essentially a linear bias dependence out to at least +12 volts.

Figure 11 shows ΔV as a function of 5 keV electron fluence for a sample with a 5000 Å oxygen oxide irradiated at several bias levels. This sample had been annealed at 300°C prior to being irradiated. Figure 11 is drawn to the same scale as that of Fig. 7 in terms of the effective density of induced charge or the density of charged states N_{ss}. In comparing N_{ss} in the 2500 Å and 5000 Å oxygen oxides, it is interesting to note that for a given fluence and bias, N_{ss} is smaller in the 5000 Å sample. This disparity can be attributed to the mean range of approximately 2000 Å for 5 keV electrons in SiO_2. Consequently, at this energy fewer holes will be generated and trapped near the Si-SiO_2 interface in the thicker sample.

A number of models have been proposed to explain the positive charge build-up in SiO_2 during irradiation. It is generally agreed that electron-hole pairs are generated by the ionizing radiation; the electrons, having a higher mobility in the oxide than holes, are swept out by the applied field leaving the less mobile holes to be trapped somewhere in the oxide. This process continues until the hole traps are saturated thereby limiting further charge build-up. A common assumption of the various models is that the charge build-up takes place very close to the oxide-silicon interface. This assumption has been verified experimentally by progressively etching away layers of oxide in samples irradiated with 1 MeV electrons at zero bias (Ref. 14) and in samples exposed to X-rays at positive bias (Ref. 15). It was found in both cases that the positive charge was trapped within about 100 Å of the Si-SiO_2 interface. One might expect that with a positive bias applied to the metal electrode during irradiation

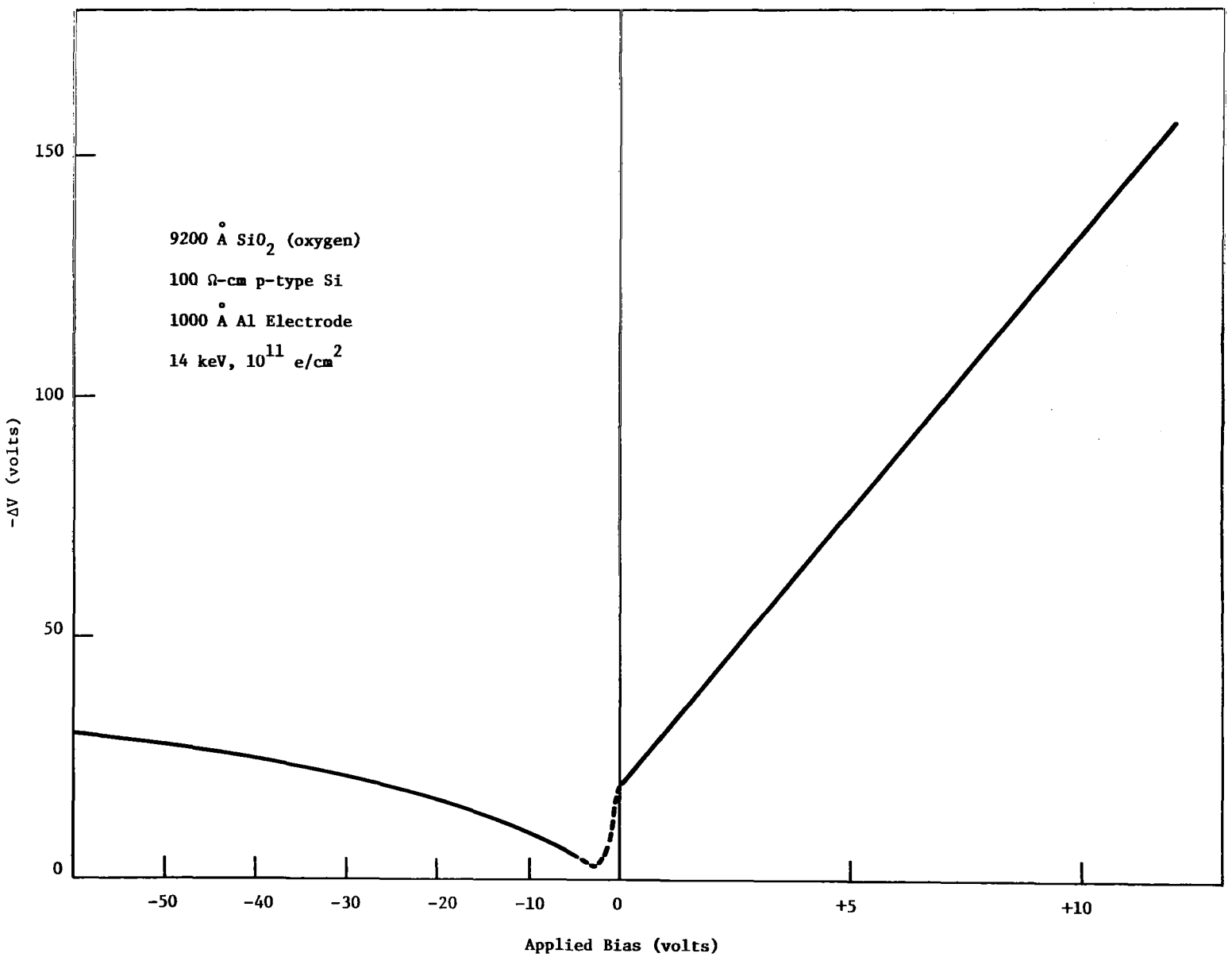

Figure 10. Charge Build-up vs. Applied Bias in 9200 Å Oxygen Oxide

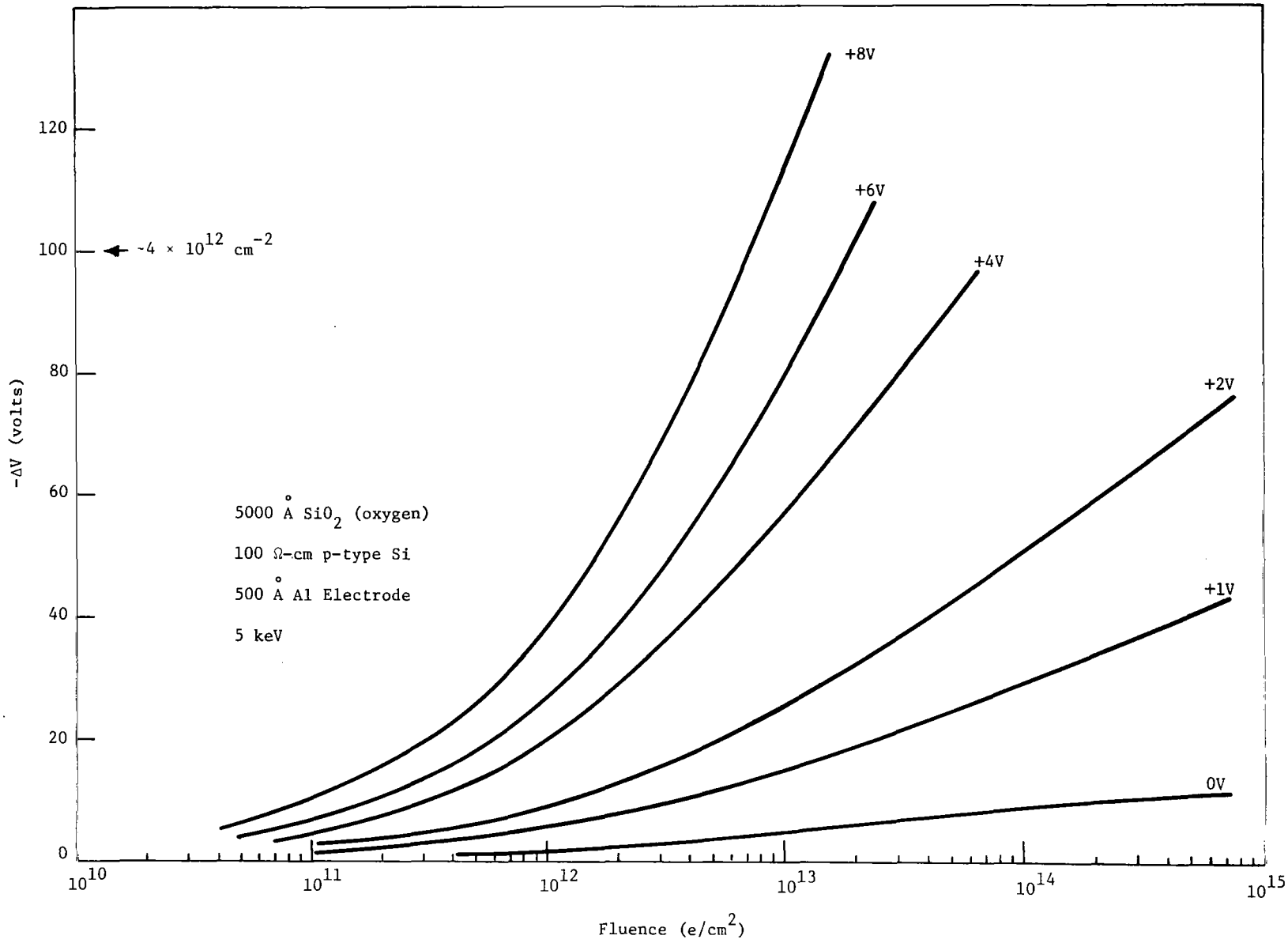

Figure 11. Charge Build-up vs. Fluence in 5000 Å Oxygen Oxide at Various Positive Bias Levels

and with most of the positive space charge collecting near the $Si-SiO_2$ boundary, a negative bias should result in a positive space charge region at the metal-SiO_2 interface. At zero external bias it becomes more difficult to predict the charge distribution since it would be a function of internal fields arising from ionic contaminants or contact potentials.

Various distributions for the positive trapped charge have been proposed to account for observed dependences of charge accumulation on bias applied during irradiation. Grove and Snow have shown that for a spatially uniform distribution of single-level traps the saturation level of induced charge is proportional to the square root of the applied bias (Ref. 15). This is essentially the same model used by Von Hippel to explain the formation of color-centers in alkali halides illuminated under bias. For the irradiated MOS structure this model says that the width of the space charge region extending from the $Si-SiO_2$ interface into the oxide increases with irradiation until it saturates at a distance determined by the applied bias. At saturation all of the applied voltage is dropped across the space charge region. In the ideal case the thickness d of the space charge region is given by

$$d = \left(\frac{2\varepsilon_{ox} V_g}{qN_t} \right)^{1/2} , \qquad (3)$$

where N_t is the trap density in cm^{-3} and V_g the applied voltage or, more precisely, the voltage dropped across the space charge region. The saturated charge per unit area, Q_{sat}, within the oxide can then be expressed as $qN_t d$. The saturated image charge per unit area induced in the silicon is then

$$Q'_{sat} = - q\left(N_{ss}\right)_{sat} = - qN_t d \left(1 - \frac{d}{2x_o}\right) , \qquad (4)$$

where x_o is the oxide thickness. Since it is assumed that $d << x_o$, Eq. (4) becomes

$$Q'_{sat} \simeq - (2\varepsilon_{ox} qN_t V_g)^{1/2} . \qquad (5)$$

This simplified model correctly predicts the saturation of induced charge with increasing exposure and the polarity of gate bias needed to produce the larger ΔV shift. Also, it provides a good approximation to some of the experimentally observed data for the dependence of Q'_{sat} on

the applied bias V. Grove and Snow observed that Q'_{sat} seemed to follow $\sqrt{V_g}$ at low biases in X-irradiated MOS structures. When the model was fitted to the experimental data it led to a trap density of about 10^{18} cm^{-3}, which agrees with that found for fused quartz by Compton and Arnold during optical studies (Ref. 16). Zaininger and Holmes-Seedle have also reported a $\sqrt{V_g}$ dependence for Q'_{sat} in the case of MOS units irradiated with 1 MeV electrons (Ref. 17).

Although the model discussed above has a number of attractive features, perhaps the majority of experimental evidence points to a linear dependence of Q'_{sat} on the bias applied during irradiation. Later data taken by Snow and co-workers (Ref. 18) along with that reported by Speth and Fang (Ref. 19) and MacDonald and Everhart (Ref. 20) indicates that Q'_{sat} more closely follows a linear voltage dependence. There are several distributions of charge in the oxide that will account for this dependence. Speth and Fang suggested that the positive charge layer is uniformly distributed within a distance d from the Si-SiO_2 interface. This distance is assumed constant and independent of applied bias. Such a model has been discussed quantitatively by Wilson, et al., (Ref. 21), who developed an expression for ΔV as a function of both applied bias and exposure time at a constant flux density. Using a one-carrier model, neglecting diffusion, and assuming that there is no trapping other than the fixed positive charge in the constant width space charge region, the image charge induced in the silicon was calculated to be

$$Q'(t) = -\frac{\varepsilon_{ox} V_g}{d}\left(\frac{2x_o}{d} - 1\right)\left[1 - \exp\left(-\beta g t\right)\right], \qquad (6)$$

where g is the generation rate in pairs cm^{-3} sec^{-1} and where

$$\beta = \frac{q d \mu_n \tau_n}{2\varepsilon_{ox} x_o}. \qquad (7)$$

The mobility-lifetime product, $\mu_n \tau_n$, for electrons in SiO_2 has been reported by Goodman to be 2.1×10^{-13} m^2/V (Ref. 22). At negative biases the positive space charge collects within a distance d of the metal-SiO_2 interface but will induce a smaller image charge in the silicon. The expression for the image charge in this case is

$$Q'(t) = -\frac{\varepsilon_{ox} V_g}{d}\left[1 - \exp\left(\beta g t\right)\right]. \qquad (8)$$

This model predicts that for large doses $Q'(t)$ exponentially approaches a saturation level Q'_{sat} which is a linear function of V_g. Also, Q'_{sat} should saturate for large values of V_g as all traps within the region of width d become saturated. Since the flux density appears only in the product gt, this model also accounts for the commonly observed independence of charge build-up versus fluence on the flux density. The major objection to this model is the difficulty in physically justifying all traps being located within a fixed distance of the $Si-SiO_2$ interface. Intuitively, one would still expect the traps to fill at least initially from the interface, which would give the square root dependence of Q'_{sat} on V_g. However, if the model is assumed to be correct and is applied to the 2500 Å steam oxide of Fig. 9, where the charge build-up is seen to have an initial linear dependence on V_g, a space charge width of about 600 Å is obtained. Using this value and assuming ΔV_{sat} would saturate at 100 volts due to trap saturation, then the trap density would be of the order of 10^{18} cm^{-3}. The non-saturating behavior seen in most of the irradiated oxygen oxides implies trap densities at least an order of magnitude greater than this.

Two other possible trap distributions have been discussed by Snow, et al., (Ref. 18). The first assumes that the hole traps are uniformly distributed in energy within the bottom portion of the forbidden band and are spatially uniform throughout the oxide. Regardless of trap density, this model predicts the linear dependence of Q'_{sat} on V_g out to only 3 or 4 volts, after which the voltage dependence becomes parabolic. Although this seems to fit the data for the saturating steam oxide in Fig. 9, a linear relationship has been observed out to 9 volts (Ref. 18). For small applied voltages, the saturated charge given by this model is

$$Q'_{sat} = - (q\varepsilon_{ox}N_{tE})^{1/2} V_g , \qquad (9)$$

where N_{tE} is the density of traps in cm^{-3} eV^{-1}. The charge distribution decays exponentially from the interface with a characteristic length

$$L = \left(\frac{\varepsilon_{ox}}{qN_{tE}}\right)^{1/2} , \qquad (10)$$

which is independent of applied voltage in the linear voltage region. Application of this model to the steam oxide of Fig. 9 yields a trap density of approximately 6×10^{16} cm^{-3} eV^{-1} and a characteristic space charge length of 600 Å. This trap density is too small to account for

the continuing rate of charge build-up in this sample. The displacement ΔV would have to saturate at 35 volts when all traps within the bottom 4 eV of the forbidden band of this 2500 Å sample were occupied.

The other distribution which gives a linear voltage dependence is a distribution in which the space charge is confined to a region of width d at a distance x_1 away from the $Si-SiO_2$ interface where $d << x_1$. Here the saturated charge is simply

$$Q'_{sat} = \frac{\varepsilon_{ox} V_g}{x_1} . \qquad (11)$$

It was suggested that the absence of ionized traps in the region adjacent to the interface could result either from a low trap density or from a high concentration of defects (Ref. 18). The latter possibility was explained by the defects causing the oxide to become more conductive thereby allowing electrons to move from the silicon and neutralize the trapped holes. However, one difficulty with this hypothesis is that electrons injected into the oxide from the silicon would still need to overcome a barrier energy of approximately 4.25 eV. Since this process proceeds as the logarithm of the elapsed time, as will be shown in Sec. IV, considerable time would be required for significant charge neutralization in region x_1. No explanation has been suggested for a reduced density of traps adjacent to the interface and, indeed, the lack of ionized traps adjacent to the interface does not seem to be supported by experimental evidence.

Each of the four steady state charge distributions discussed are depicted in Fig. 12 for several values of applied bias. The distribution of Fig. 12(a) gives the square root dependence of Q'_{sat} on applied bias and the other three result in a linear dependence.

All of the theory which has been proposed so far to characterize the charge build-up in the irradiated MOS structure has been based on a one-carrier model. It has been assumed that the hole mobility in SiO_2 is relatively small compared to that of electrons and consequently any possible motion and concentration gradients of free holes in the oxide has been neglected during charge build-up. In addition, most of the models describe only the steady state or equilibrium charge as a function of bias applied during irradiation. While the features of several of these models are appealing, no single model seems to satisfactorily describe the observed charge build-up as a function of time or account for the various ways in which saturated charge density depends on applied bias.

Although the respective mobility-lifetime products of electrons and holes in SiO_2 has been reported by Goodman to be approximately 2.1×10^{-13} m^2/V and 10^{-14} m^2/V, it is conceivable that the charge build-up process

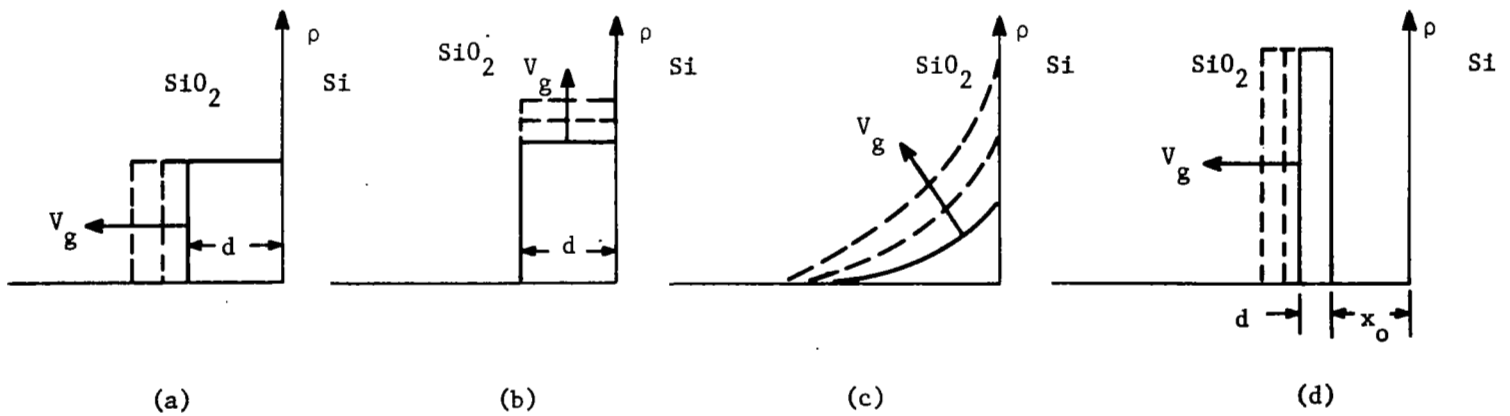

(a) spatially uniform single level traps

(b) uniform charge build-up within region adjacent to interface

(c) spatially uniform traps uniformly distributed in energy

(d) no charge build-up in region immediately adjacent to interface

Figure 12. Steady State Oxide Charge Distributions (Ref. 18)

could be influenced by the motion and distribution of free holes as well as that of free electrons generated in the oxide by the incident radiation. Therefore, a complete analysis of the problem should include these effects. It is also highly desirable to be able to incorporate into a model different electron and hole trap distributions as well as several nonuniform carrier generating functions approximating the energy dissipated by nonpenetrating electrons in various oxide thicknesses.

Any two-carrier models incorporating the above features would, of course, be sufficiently complex to require the use of a computer to solve the resulting equations. The equations developed to characterize a two-carrier model and the problems experienced in the computer solution are described in the Appendix.

Effect of Beam Energy and Oxide Thickness

Figures 13, 14, and 15 show ΔV as a function of fluence with energy as the parameter for samples having oxygen-grown oxides of 2500 Å, 5000 Å, and 9200 Å, respectively. The applied bias was held constant during the series of irradiations made on each sample. It is seen that for each oxide thickness the charge build-up increases with energy until some energy E_{max} where the induced charge reaches a maximum. Further increase in beam energy causes the charge build-up to fall off. Figure 14 also includes results from the high energy irradiations made on 5000 Å samples. Even at beam energies of 200 keV and 1 MeV the charge build-up continues to fall off from the peak reached at 10 keV. It is also noted that 200 keV and 1 MeV curves are essentially parallel to the 7, 10, and 20 keV curves or merely displaced toward a higher fluence.

It is interesting to compare the energy dependence of the induced charge in the three samples with the energy dissipation curves for monoenergetic electrons. These curves, shown in Fig. 16, were plotted for SiO_2 using general range-energy relationships which have been summarized by Schumacher and Mitra (Ref. 23). Vertical bars have been drawn at distances corresponding to the depth of the Si-SiO_2 interface from the top surface of the aluminum electrode for each of the three samples. Since the range of penetration of 5-100 keV electrons is a function of the density of the material and not the atomic number, the aluminum electrode thickness, increased by 15% to allow for the higher density of aluminum, has been added to that of the oxide. It is apparent from Fig. 16 that the beam energies which yield maximum energy dissipation at the Si-SiO_2 interface correspond to E_{max} for each of the three oxide thicknesses as indicated in Figs. 13 through 15. Also, for a given sample the relative effectiveness of the various primary electron energies in inducing oxide charge corresponds to the relative energy dissipation per unit path length at the oxide-silicon

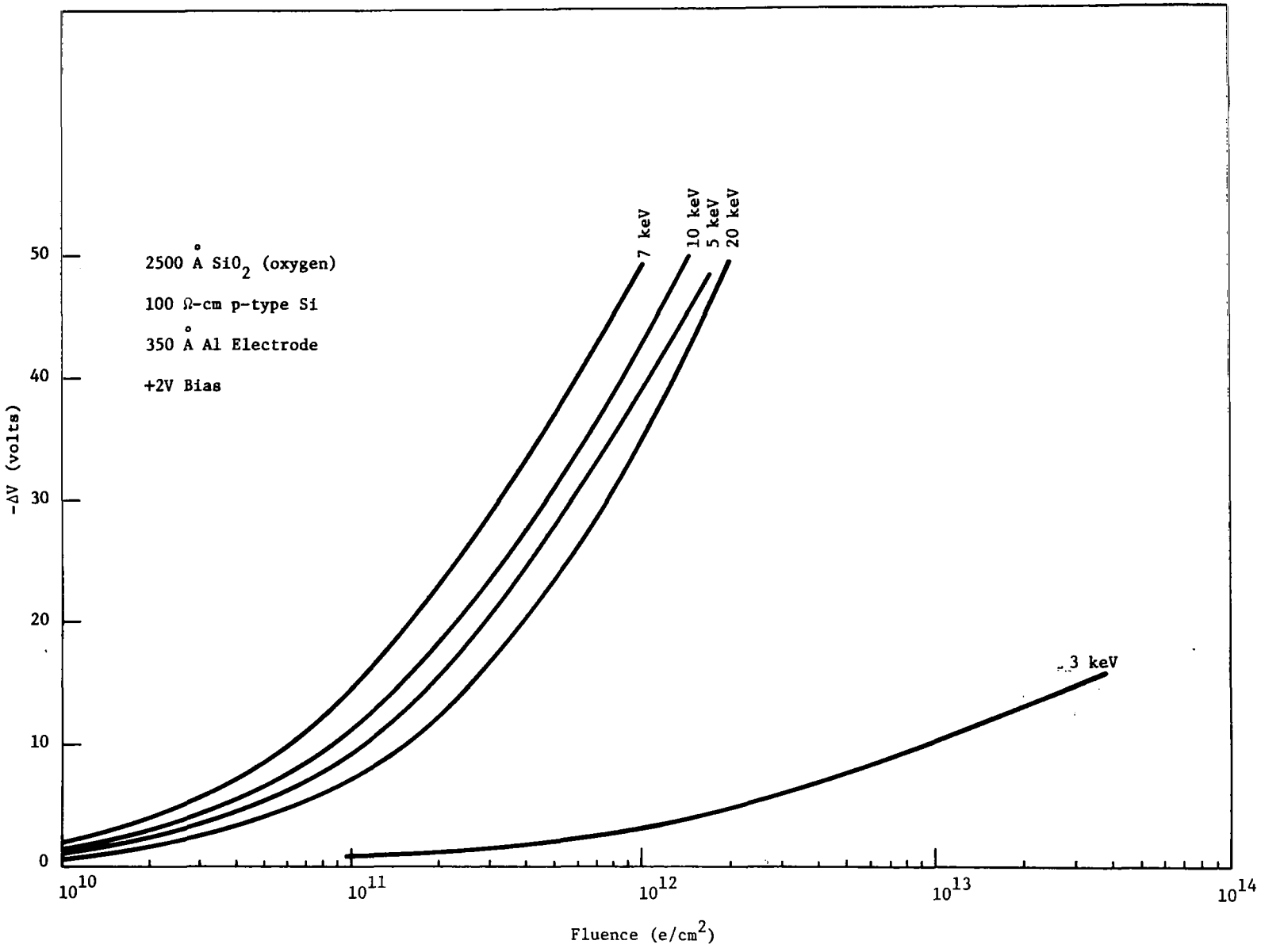

Figure 13. Charge Build-up vs. Fluence for 2500 Å Oxygen Oxide at Various Beam Energies

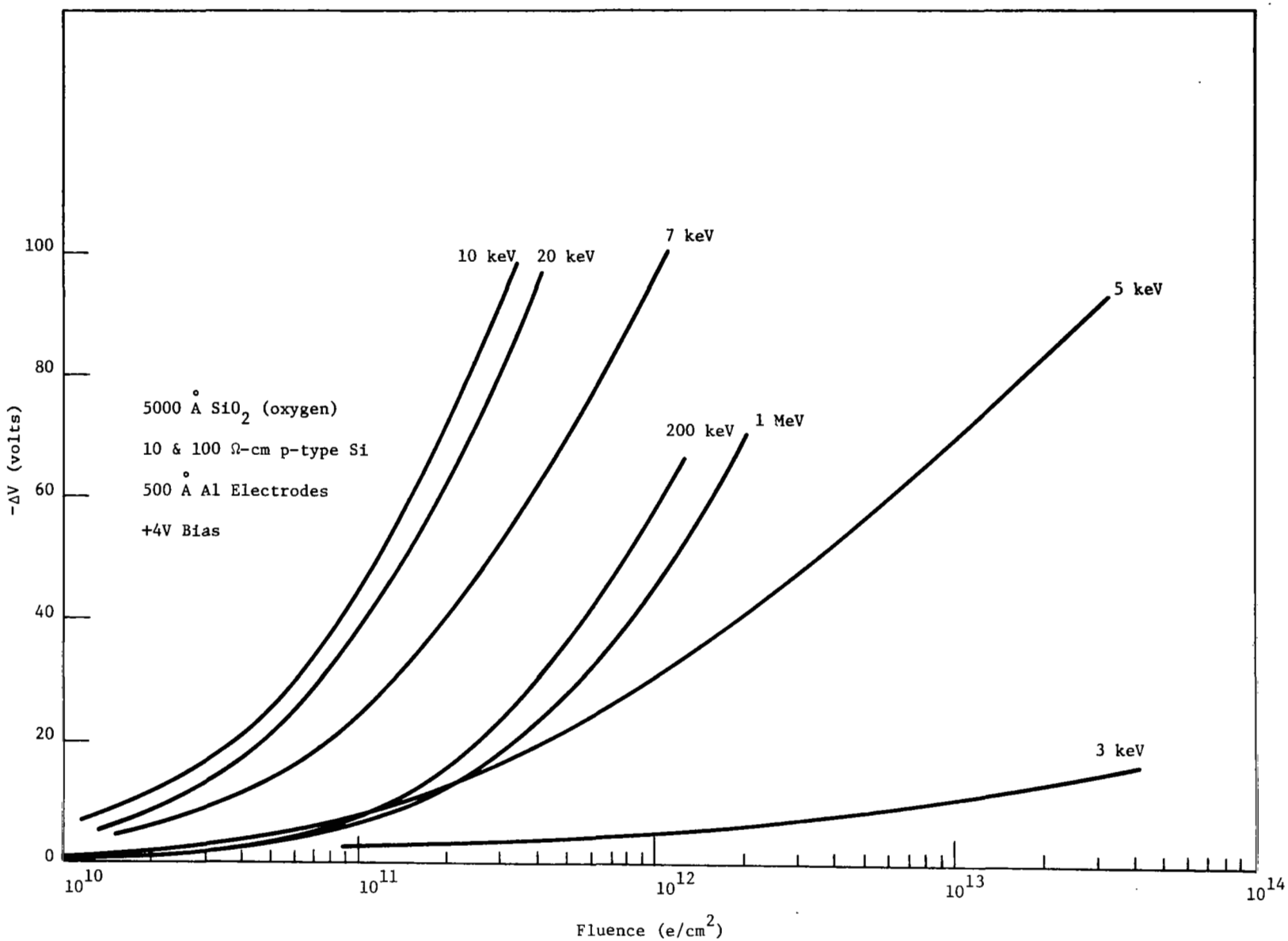

Figure 14. Charge Build-up for 5000 Å Oxygen Oxide at Various Beam Energies

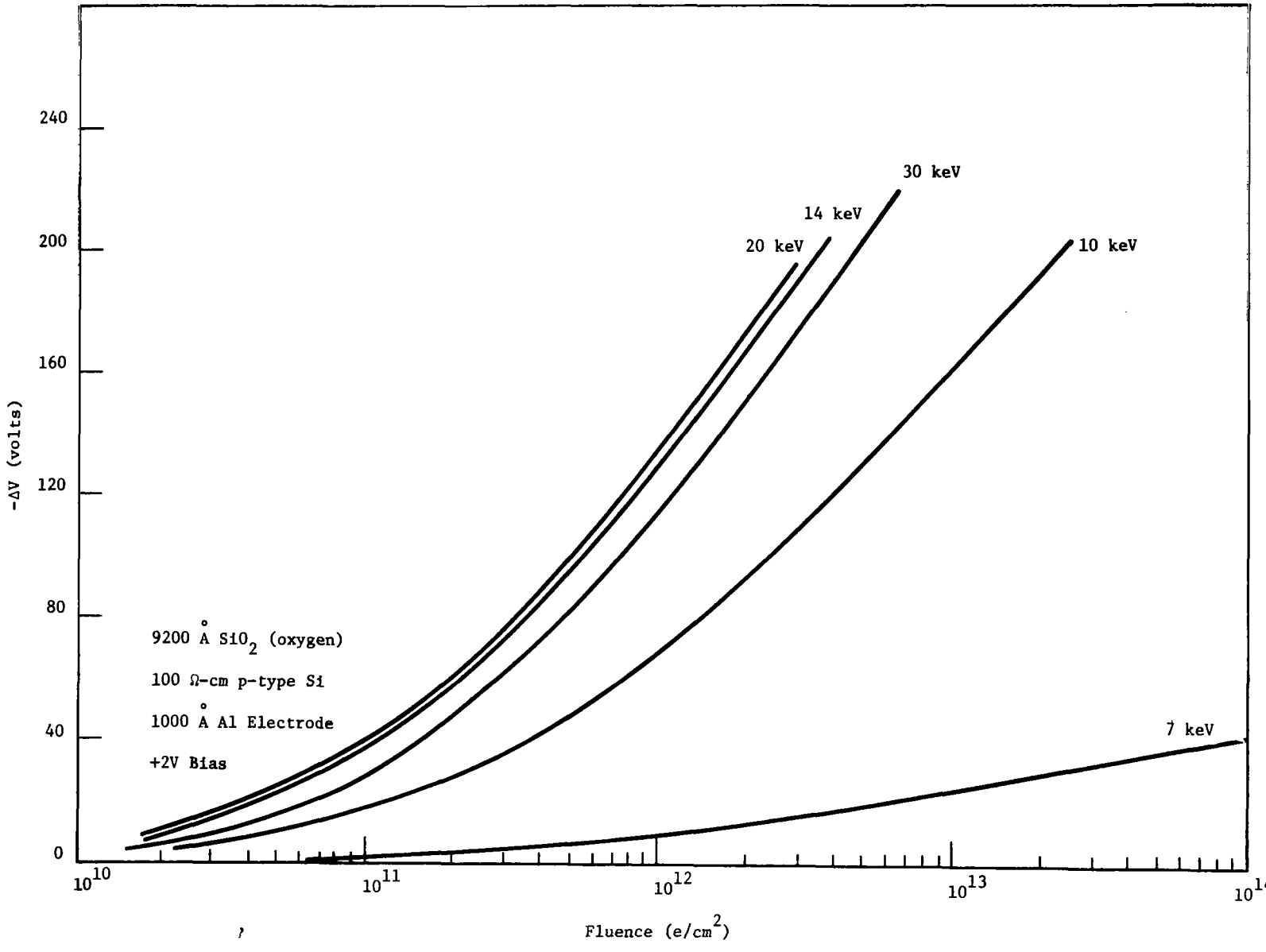

Figure 15. Charge Build-up for 9200 Å MOS Sample Irradiated at Various Energies

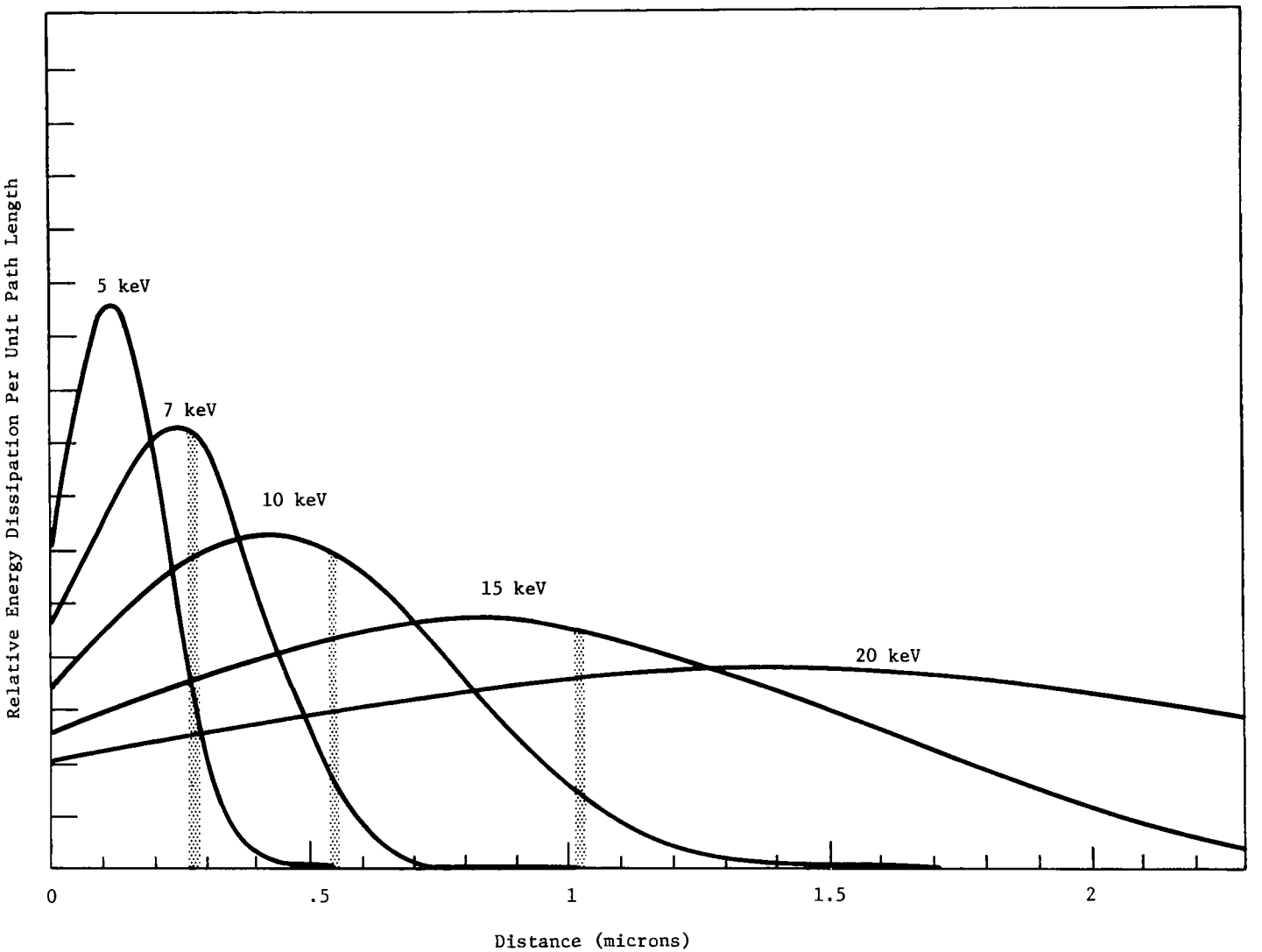

Figure 16. Energy Dissipation Curves for Monoenergetic Electrons in Silicon Dioxide

interface as indicated in Fig. 16. This supports the logical assumption that at positive biases ionizations occurring in the region adjacent to oxide-silicon interface are the most effective in introducing trapped positive charge into this region where the trapped charge produces a maximum voltage displacement ΔV. It cannot be concluded from this data that ionizations occurring elsewhere in the oxide do not result in trapped positive charge somewhere in the oxide.

Figure 17 compares the maximum rates of charge build-up observed in the three oxide thicknesses. Each sample was irradiated at the appropriate primary beam energy E_{max} and at a bias of +2 volts. The ordinate has been normalized to charge per unit area to facilitate a comparison between the samples of differing thickness. It is noted that the build-up rate is largest for the 2500 Å sample and smallest for the 9200 Å sample, corresponding to the relative energy dissipated at the oxide-silicon interface in each sample at the appropriate beam energy E_{max} as indicated in Fig. 16. An interesting observation from Fig. 17 is that the rate of charge build-up at a particular level of applied bias is essentially independent of the oxide thickness provided, of course, that the energy dissipation or carrier generating function at the oxide-silicon interface is kept constant. This is also illustrated by the same charge induced in 2500 Å and 5000 Å oxide samples irradiated at 10 keV and +2V bias, as shown in Figs. 13 and 17, respectively, where the ordinates have been plotted to the same charge density scale. According to the dissipation curves of Fig. 16, the same energy is dissipated at the oxide-silicon interface in both samples. This observation lends support to a model in which the trapped charge rapidly accumulates in a narrow region much less than and independent of the total oxide thickness. The electric field approaches zero everywhere in the oxide except in the narrow space charge region and thus becomes a function only of applied bias which is independent of the total oxide thickness.

The series of high energy irradiations (200 keV and 1 MeV) produced results consistent with those obtained at lower energies. A total of fourteen samples, most of which had 5000 Å oxides grown in oxygen, were irradiated at various bias levels. The charge build-up at 1 MeV was slightly less than at 200 keV for a given level of applied bias as shown in Fig. 14. At both 200 keV and 1 MeV the induced charge was considerably smaller than at the lower electron energies where more energy can be absorbed by the oxide. No difference was found in the dependence of charge build-up on applied positive bias in oxides irradiated at high and low energies. Figure 18 shows the voltage displacement as a function of fluence for 5000 Å oxygen oxides irradiated at 200 keV under various bias conditions. As observed at lower energies, steam oxides exposed at both 200 keV and 1 MeV under positive bias showed less charge accumulation than oxygen oxides irradiated under the same conditions. Samples were exposed at flux densities of 10^9 and 10^{10} electrons per cm^2 per sec, but no significant

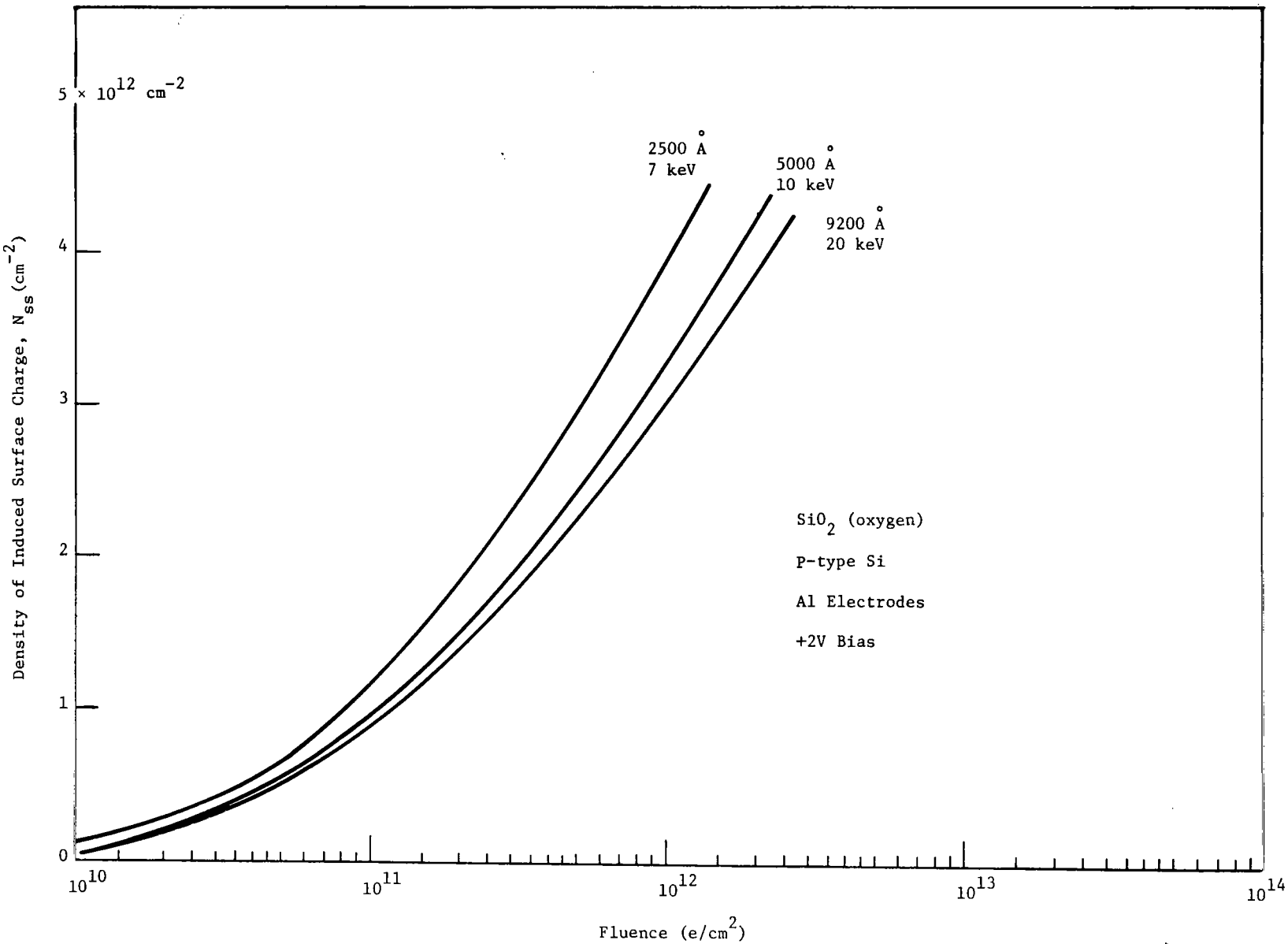

Figure 17. Comparison of Maximum Charge Build-up Rates in Three Thicknesses of Oxygen Oxides

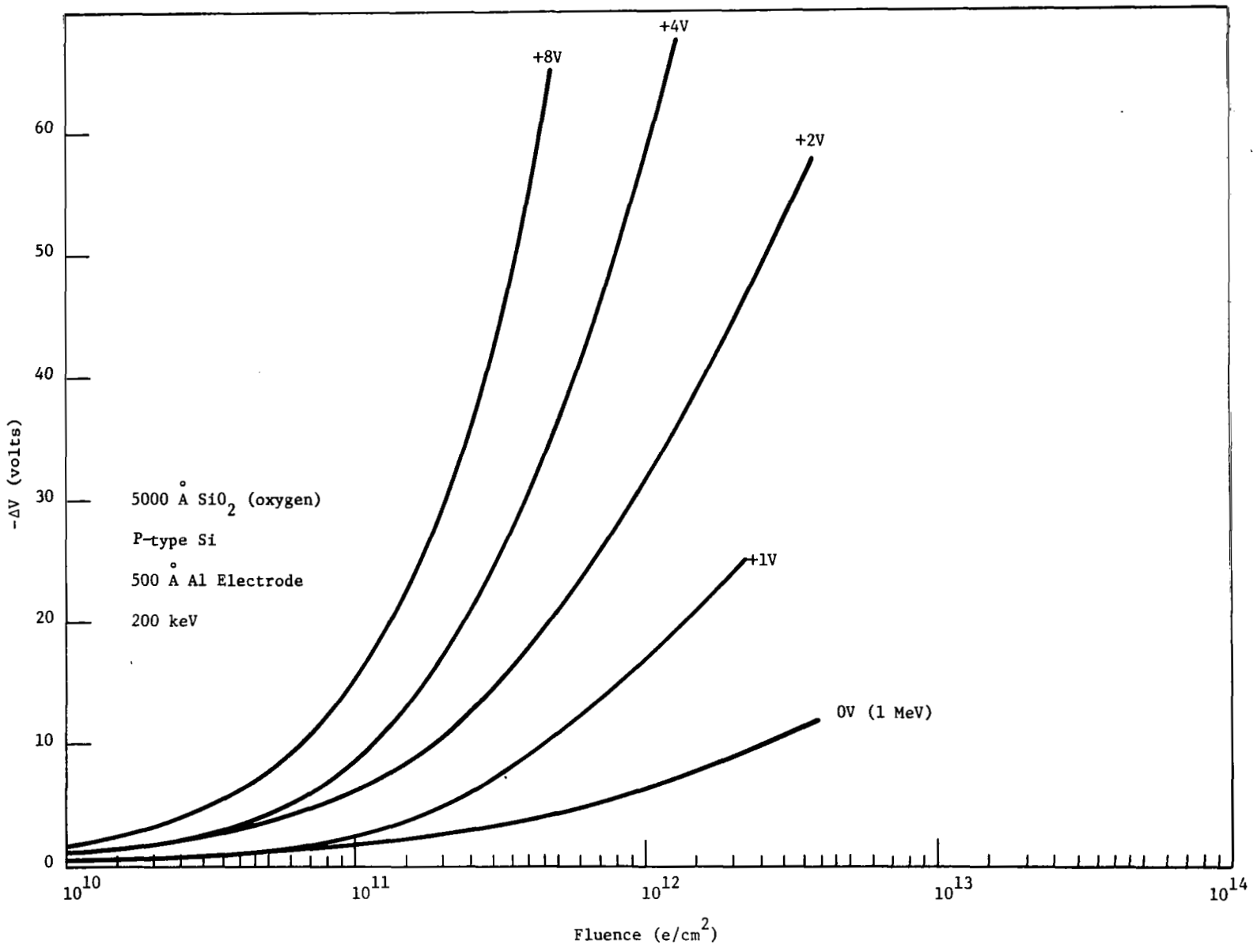

Figure 18. Charge Build-up in 5000 Å Oxygen Oxides Irradiated at High Energy

rate dependence of charge build-up was detected. Again, the induced charge was found to be smaller in samples which had previously undergone a 300°C anneal.

Effect of Electrode Material and Thickness

Charge build-up in an electron-irradiated MOS structure is dependent on the number of primary electrons passing through the metal electrode with sufficient energy to penetrate the oxide. Since secondary electrons have insufficient energy (< 20 eV) to allow oxide penetration, the secondaries emitted from the metal electrode should have little or no effect on the induced charge. However, the fraction of backscattered electrons will be reflected in a corresponding decrease in induced oxide charge. The backscattering coefficient for aluminum irradiated at energies above 5 keV ranges from a maximum of 0.15 in the bulk down to less than .05 in 500 Å film (Ref. 13) and is therefore not too significant. However, for higher Z metals such as silver, gold, and platinum, the backscattering coefficient may reach as high as 0.4, which is an appreciable fraction of the incident particles.

To study the effect of aluminum electrode thickness on the induced charge, an MOS sample having an oxygen-grown oxide of about 2100 Å was prepared with an initial electrode thickness of 500 Å. Following irradiation and the subsequent removal of the induced charge, an additional thickness of aluminum was evaporated over the original electrode. The sample was re-irradiated and the process repeated until a total electrode thickness of 10,000 Å was reached. Figures 19 and 20 show the results of these irradiations at 5 and 10 keV, respectively. If one compares this data with the 5 and 10 keV energy dissipation curves of Fig. 16, bearing in mind that approximately 15% should be added to the actual electrode thickness to allow for the increase in mass-thickness of aluminum over SiO_2, it can be seen that charge build-up is dependent on the energy dissipated in the oxide by primaries penetrating the aluminum electrode. As the electrode thickness approaches the maximum range of the incident primaries, ΔV becomes zero. The maximum range in aluminum of the 5 keV electrons is about 4000 Å, while the 10 keV particles have a maximum range of the order of 12,000 Å. Upon examination of the 10 keV dissipation curve of Fig. 16, one might expect a 2100 Å sample irradiated at this energy to show an increase in charge build-up as the electrode thickness increased from 500 to 2000 Å, since this would produce greater energy dissipation in the oxide. However, any small increase in energy dissipation in the oxide as the electrode thickness was increased in this range has probably been offset by a corresponding increase in the backscattering coefficient, thereby causing the charge build-up to be about the same for 500 Å, 1000 Å, and 2000 Å aluminum electrode thicknesses.

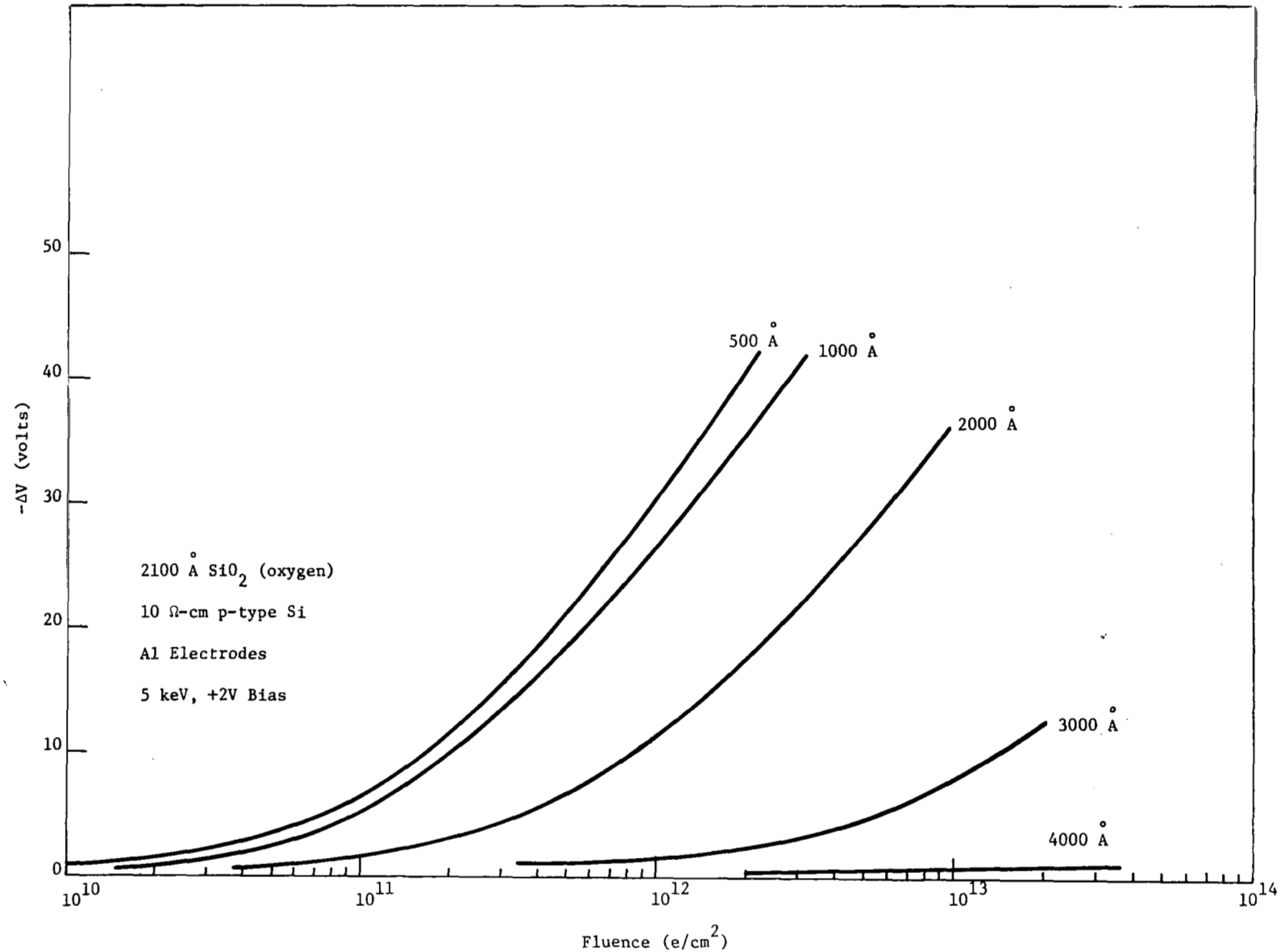

Figure 19. Charge Build-up vs. 5 keV Electron Fluence as a Function of Aluminum Electrode Thickness

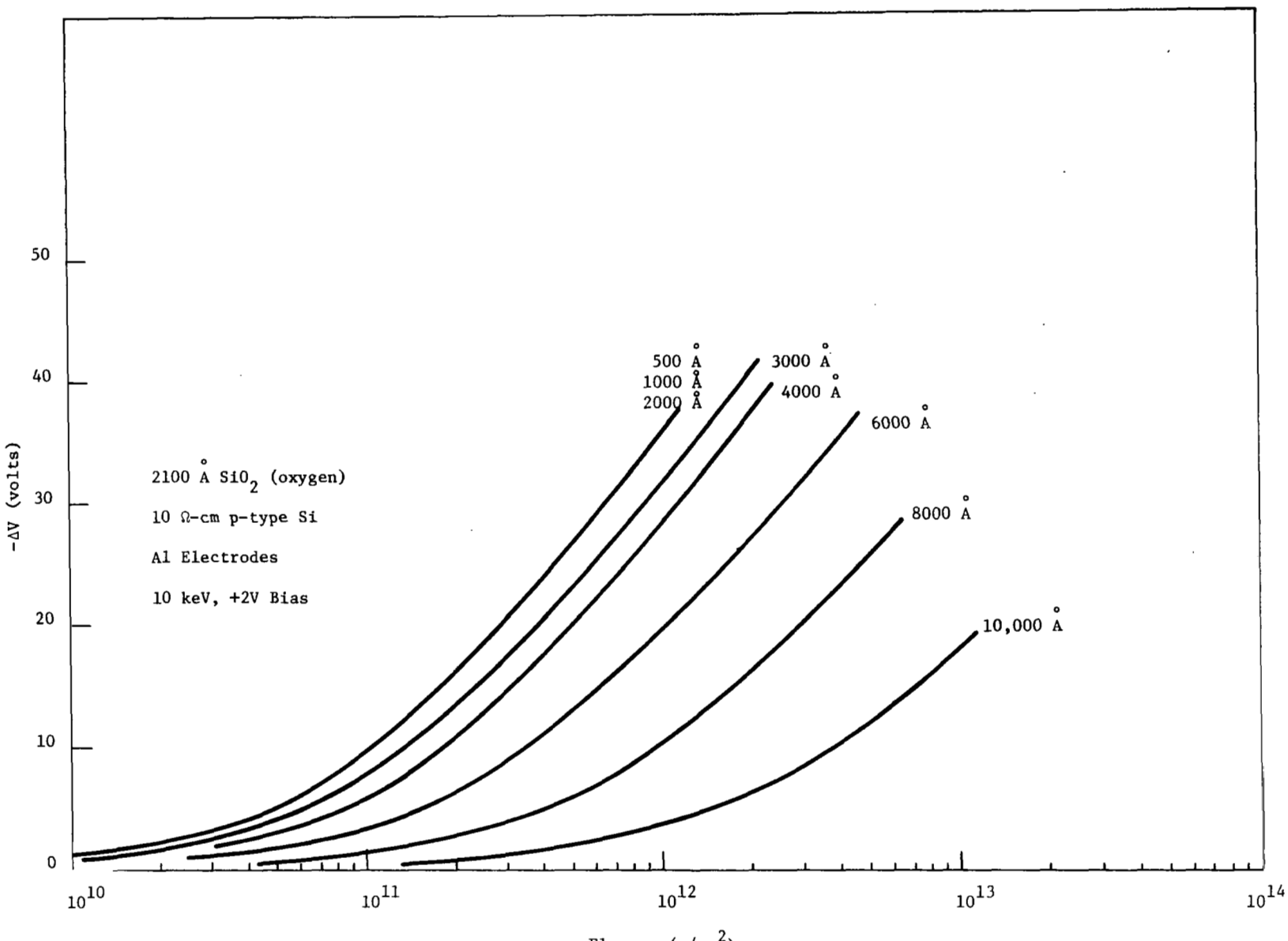

Figure 20. Charge Build-up vs. 10 keV Electron Fluence as a Function of Aluminum Electrode Thickness

A comparison of charge accumulation in samples with 500 Å aluminum, gold, and silver electrodes irradiated at 5 keV is shown in Fig. 21. The oxides were prepared simultaneously in an oxygen environment and have a thickness of approximately 2700 Å. Because of the lower mass-thickness of the aluminum electrode this sample has a significantly higher charge build-up than in the two samples with the heavier electrode materials. Since the gold electrode has a mass-thickness of about 95 mg/cm^2 as compared to 52 mg/cm^2 for the silver electrode, one would not expect to see nearly the same charge induced in both samples. To remove any possible sample-to-sample variation from the experiment, the 500 Å silver electrode was etched off and replaced with 500 Å of gold. This sample was re-irradiated and the charge build-up was again found to be about the same as with the previous electrode. Assuming that the electrode thicknesses were monitored correctly, the only apparent explanation for the charge build-up being about equal with the two type electrodes is that the backscattering fraction for 5 keV electrons is greater for 500 Å of gold than for the same thickness of silver and thus compensates for the higher mass thickness of gold. The backscattering coefficient at low electron energies has been reported by Sternglass to be somewhat higher for bulk gold than for bulk silver (Ref. 24).

Effect of Other Oxide Characteristics

A number of oxide-related parameters were varied during the course of this work to determine which factors affected the radiation sensitivity of SiO_2. In addition to the influence of the factors cited previously such as method of oxide preparation and thermal annealing of completed samples, the effects of substrate resistivity and oxide contamination were studied. Also several samples having oxides passivated with a layer of phosphosilicate glass were prepared and irradiated. The dependence or independence of charge build-up on these properties will be discussed in the following paragraphs.

Method of Thermal Oxidation. - The lower radiation sensitivity for a 2500 Å steam oxide as compared with an oxide of the same thickness prepared in oxygen was illustrated in Figs. 7 and 8 and has been discussed briefly. This data agrees with the work of Zaininger who has reported a larger charge build-up in 1000 Å oxygen oxides than in 1000 Å steam oxides when irradiated with 1 MeV electrons (Ref. 14). To determine if this difference in radiation sensitivity existed in thicker oxides, 11,000 Å steam oxides were prepared and irradiated. The charge build-up in these samples as a function of fluence was found to be almost identical with that seen in the 9200 Å oxygen samples irradiated earlier. Unlike the

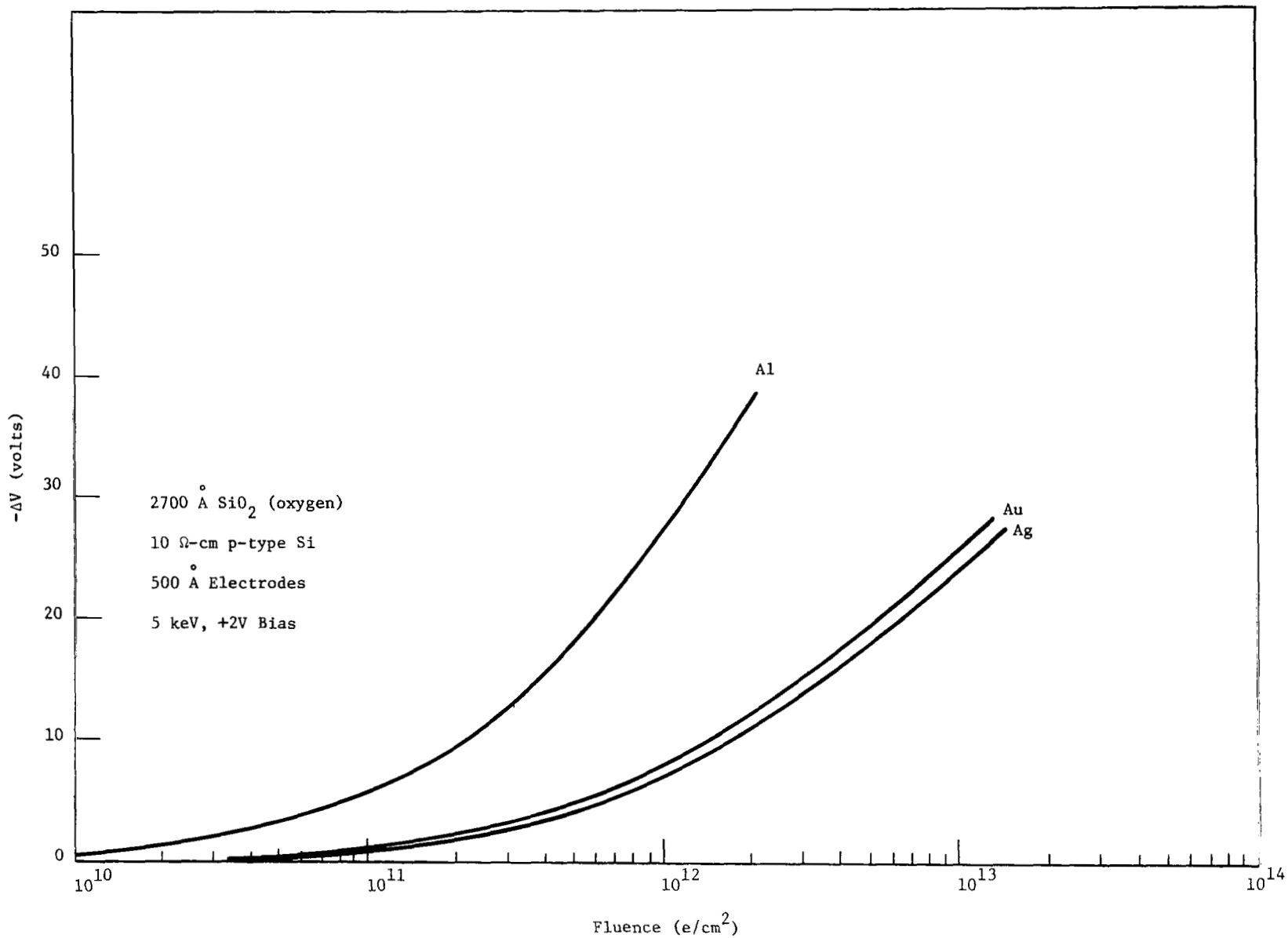

Figure 21. Charge Build-up vs. Fluence as a Function of Electrode Material

2500 Å steam oxides the thicker steam oxides showed no tendency to saturate. Although there was a slight reduction in the charge build-up for a sample which had been annealed at 300°C, the radiation sensitivity of both the annealed and unannealed thick steam oxides was essentially the same as that seen in the oxygen oxides. However, when 5000 Å steam oxides were irradiated at 200 keV, an appreciably lower charge density was induced than in the oxygen samples exposed under the same conditions. A reduction in charge build-up by a factor of 2 or 3 at a fluence of 10^{12} e/cm^2 was observed; but unlike the 2500 Å steam oxides, there was no indication of saturation in the charge build-up in the 5000 Å steam oxides.

It would appear from the available data that in the thickness range below 5000 Å steam oxides are definitely less sensitive to radiation than oxygen oxides. It is not readily apparent whether this reduced sensitivity is directly a function of thickness and therefore limited to the thinner oxides or whether some thickness-related oxidation parameter is involved.

Post Oxidation Anneal. - The charge induced in three different 5000 Å oxygen oxide samples irradiated at 5 keV at biases of +2 and +8 volts is compared in Fig. 22. As in the case of the steam oxide of Fig. 8, a greater charge build-up takes place in the two unannealed samples (1) and (2) than in sample (3) which was annealed at 300°C prior to irradiation. It has been consistently observed during this work that samples annealed at about 300°C for several minutes show a lower charge build-up during irradiation than do the unannealed samples, although the difference in radiation sensitivity between annealed and unannealed samples is not always as large as that depicted in Fig. 22. A reduction of hole traps in the oxide during the post oxidation anneal seems likely. One should be able to achieve the same result by reducing the oxide temperature following oxidation at a carefully controlled rate. If the radiation sensitivity of SiO_2 is a function of the post oxidation cooling rate, this may explain the different sensitivities observed among some of the steam oxides.

Substrate Resistivity. - Figure 22 also compares the charge build-up in samples fabricated on different resistivity substrates. Sample (1) was prepared on a 100Ω-cm p-type substrate and sample (2) on a 10Ω-cm substrate of the same type. When irradiated at the lower bias, the difference between the ΔV versus fluence curves is small. At the higher bias the difference is somewhat larger; however, it is believed that the disparity in charge build-up between these two samples did not result from the difference in substrate resistivity but arose from differences in the radiation sensitivities of the two unannealed samples having oxides grown separately. No consistent difference in the radiation sensitivity of samples has been observed during this work that could be traced to substrate resistivity.

Several samples with thin oxides on 100Ω-cm n- and p-type substrates were prepared and irradiated to determine if the substrate type affected

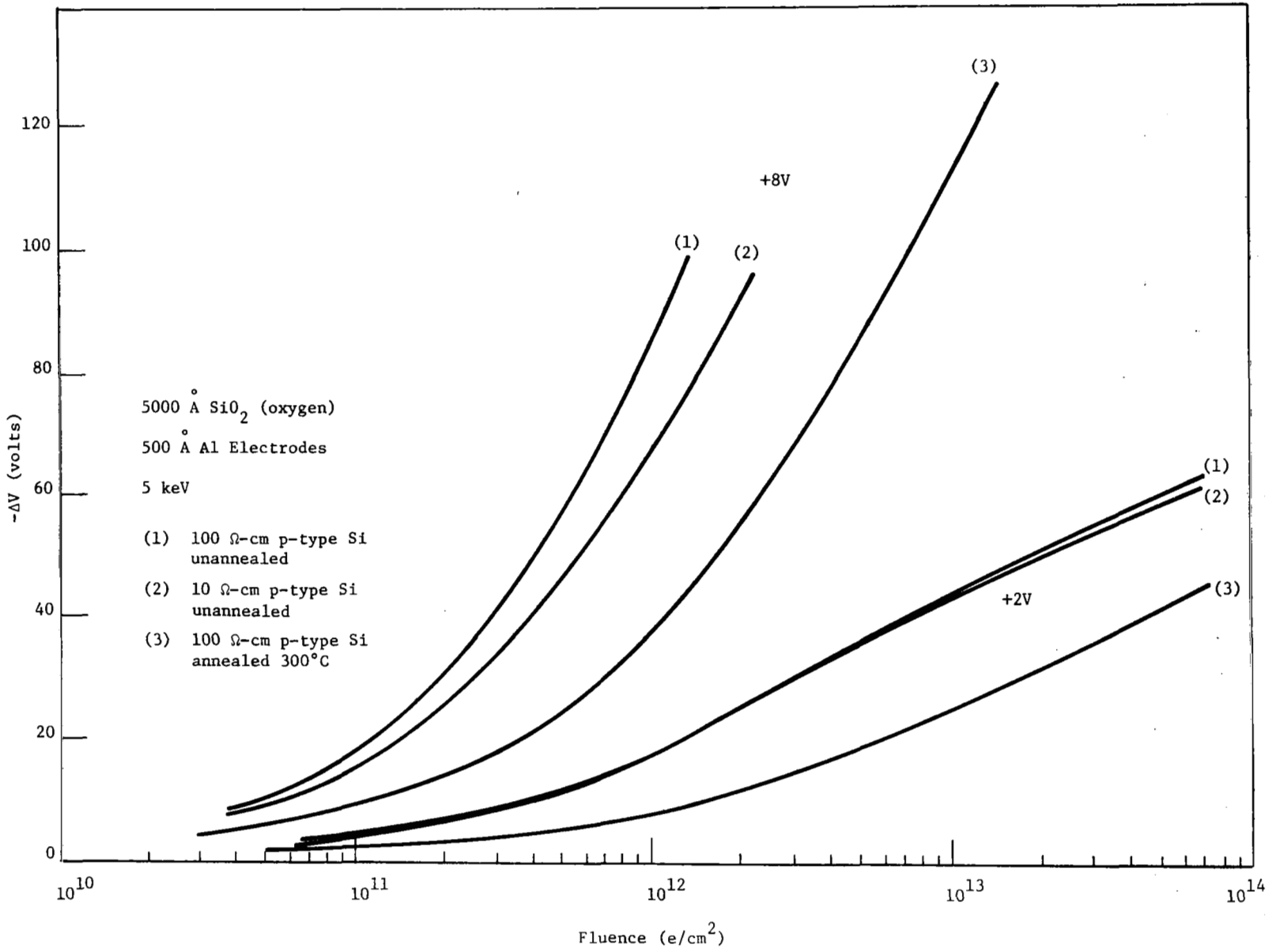

Figure 22. Comparison of Charge Build-up in Annealed and Unannealed Oxides

the induced charge; however, the oxides were leaky and the results of the experiment inconclusive.

Oxide Contamination and Surface Passivation. - Because of the possibility that sodium may act as a network modifier in SiO_2, the presence of this impurity could conceivably have some effect on the density of hole traps in the oxide and a corresponding influence on its radiation sensitivity. To find whether sodium had any effect on the charge build-up of an irradiated oxide, several samples were contaminated prior to metalization with a NaOH or NaCl solution. Following electrode deposition the samples were irradiated and the induced charge characterized as a function of fluence. The space charge was then annealed and the sample subjected to a temperature-bias treatment such that the mobile sodium impurity ions were drifted into the oxide toward the oxide-silicon interface. The ion density at the interface was determined from the C-V displacement. The sample was then re-irradiated and the charge build-up compared with that taking place before drift and that in non-contaminated control samples having a low initial density of mobile impurity ions. No significant difference was observed in the charge build-up in samples with sodium ion concentrations present at the oxide-silicon interface ranging from 2×10^{11} cm^{-2} to 2×10^{12} cm^{-2}. This experiment, which is consistent with all other data, indicates that sodium does not have an effect on the radiation sensitivity of SiO_2 when present in levels of 2×10^{11} cm^{-2} or higher.

Since phosphorus-treated oxides have been reported to show improved stability and a lower density of mobile ions, the effect of this treatment on the radiation sensitivity of SiO_2 was investigated. Two samples, one with a 2500 Å oxygen oxide and the other having a 5000 Å oxide of the same type, were subjected to a P_2O_5 diffusion immediately following oxidation. An aluminum electrode was then evaporated onto each sample. The thinner sample when irradiated at 5 and 10 keV showed the same charge build-up as that observed in non-treated control samples. However the 5000 Å oxide when irradiated at 200 keV was noticeably less sensitive to radiation than the 5000 Å control samples. Following an anneal of the induced charge, the sample was irradiated at 10 keV; again, a significantly smaller positive charge build-up was observed in this sample than in the non-treated oxides or in the 2500 Å phosphorus-treated oxide. The only outstanding difference between the two treated samples was that the 2500 Å sample had a mobile ion density of 2×10^{11} cm^{-2} whereas the 5000 Å sample only had 9×10^{10} mobile ions per cm^2. Therefore, the possibility remains that a reduction in the sodium concentration below 2×10^{11} cm^{-2} might decrease the radiation sensitivity of SiO_2. However, since no other phosphorus-treated samples

nor any other non-treated samples having ionic concentrations less than 2×10^{11} cm^{-2} were prepared and irradiated, no definite conclusions can be drawn from the above experiment. In view of the lower radiation sensitivity exhibited by many steam oxides which were usually "dirtier" than the oxygen oxides, it appears that some structural characteristic of the oxide has a more pronounced effect on its radiation sensitivity than the presence of sodium or other ionic impurities.

SECTION IV

RELEASE OF TRAPPED CHARGE

Introduction

Several techniques have been found effective in removing or reducing the radiation-induced trapped charge in SiO_2. In addition to the most obvious method of annealing at elevated temperatures, it has been noted that electron irradiation at small negative sample biases was very useful in removing or reducing radiation induced charge trapped near the oxide-silicon interface. Optical annealing of the trapped charge has also been accomplished, although this is perhaps the least effective means of charge removal.

Irradiated samples have been found to be very stable at room temperature with only a small fraction of the induced charge decaying within a period of days or weeks. From the observed behavior of this trapped charge, one would expect the traps to be deep within the SiO_2 forbidden band, which has been reported by Williams to be about 8 eV (Ref. 25). If for example half of the trapped charge were released within a period of 2 weeks at room temperature, the trapped holes would have to be within at least 1 eV of the valence band assuming a single trap level. Since a decay rate this large has not been observed at room temperature, most of the trapped positive charge is assumed to lie in levels deeper than 1 eV.

In this section the technique of charge removal by electron irradiation will be discussed. Also, the results of thermal and optical annealing experiments designed to obtain information on the nature of the trapped charge will be covered. Finally, charge release in evaporated SiO will be compared to that in thermally grown SiO_2.

Radiation Annealing

It has been possible to remove completely all observable radiation-induced space charge in some samples by the technique of radiation annealing. In other samples radiation annealing is less effective and some residual space charge is left in the oxide. It has not been possible to correlate residual space charge with oxide properties or previous oxide history; however, it has been found that the residual charge in any particular sample can be reduced to a minumum by irradiating at an optimum sample bias and electron beam energy. The most effective sample bias is generally in the range from -1 to -3 volts, which was seen in Figs. 9 and 10 to produce minimum space charge formation. The resulting electric field in the oxide causes the generated electrons to drift toward the oxide-silicon interface where they recombine or become trapped. Since the C-V curves could not be shifted to positive voltages but only back to their original pre-irradiation positions, it was concluded that the

electrons served to reduce the positive space charge through recombination and did not form a compensating negative space charge. Larger negative biases were less effective probably because of the rapid build-up of hole trapping adjacent to the metal-silicon interface.

Figures 23 and 24 show the percent charge removed as a function of fluence in 5000 Å and 9200 Å samples, respectively, with energy being the parameter. It has been observed that the positive oxide charge is usually reduced most effectively when the beam energy is selected to maximize the total energy dissipated in the oxide while minimizing that dissipated at the oxide-silicon interface. An effective beam energy can be chosen in this way from Fig. 16. A large energy dissipation in the oxide is needed to insure that an abundance of excess electrons is available to neutralize the positive charge.

It is interesting to note from Fig. 23 that at 5 keV, only about 1.2×10^{12} irradiation electrons per cm^2 are required to neutralize 3.2×10^{12} charged states per cm^2 in the oxide. The additional 2×10^{12} electrons per cm^2 needed for compensation are generated within the oxide by the incident radiation. To preserve charge neutrality in the oxide an additional 2×10^{12} holes per cm^2 must be accounted for. These surplus holes are either removed from the oxide or they become trapped near the metal-oxide interface where they are least effective in producing a C-V displacement ΔV. Assuming that these holes are trapped uniformly within a distance d of the interface, then using the maximum resolution of the measuring system of about 0.5 volt, an estimate can be obtained for d. The calculation indicates that the positive charge is trapped within approximately 100 Å of the metal interface. The value reported by Zaininger (Ref. 14) and Grove and Snow (Ref. 15) for the space charge width next to the oxide-silicon interface following irradiation at positive biases was also 100 Å.

Optical Annealing

In an effort to learn something of the nature of the trapping levels in SiO_2, optical annealing studies were conducted on irradiated MOS structures. Samples which had been prepared with 300 Å aluminum and silver electrodes were irradiated under positive bias and then exposed to light from several sources. No reduction of the space charge was detected while using either tungsten or silicon carbide sources, which cover the spectrum from approximately 0.3 to 16 microns or photon energies from 0.8 up to nearly 4 eV. Upon further reduction in wavelength using light from an ultraviolet source passed through a monochrometer, space charge anneal was first observed at energies slightly below 5 eV. However, since the threshold for photoemission of electrons from silicon into

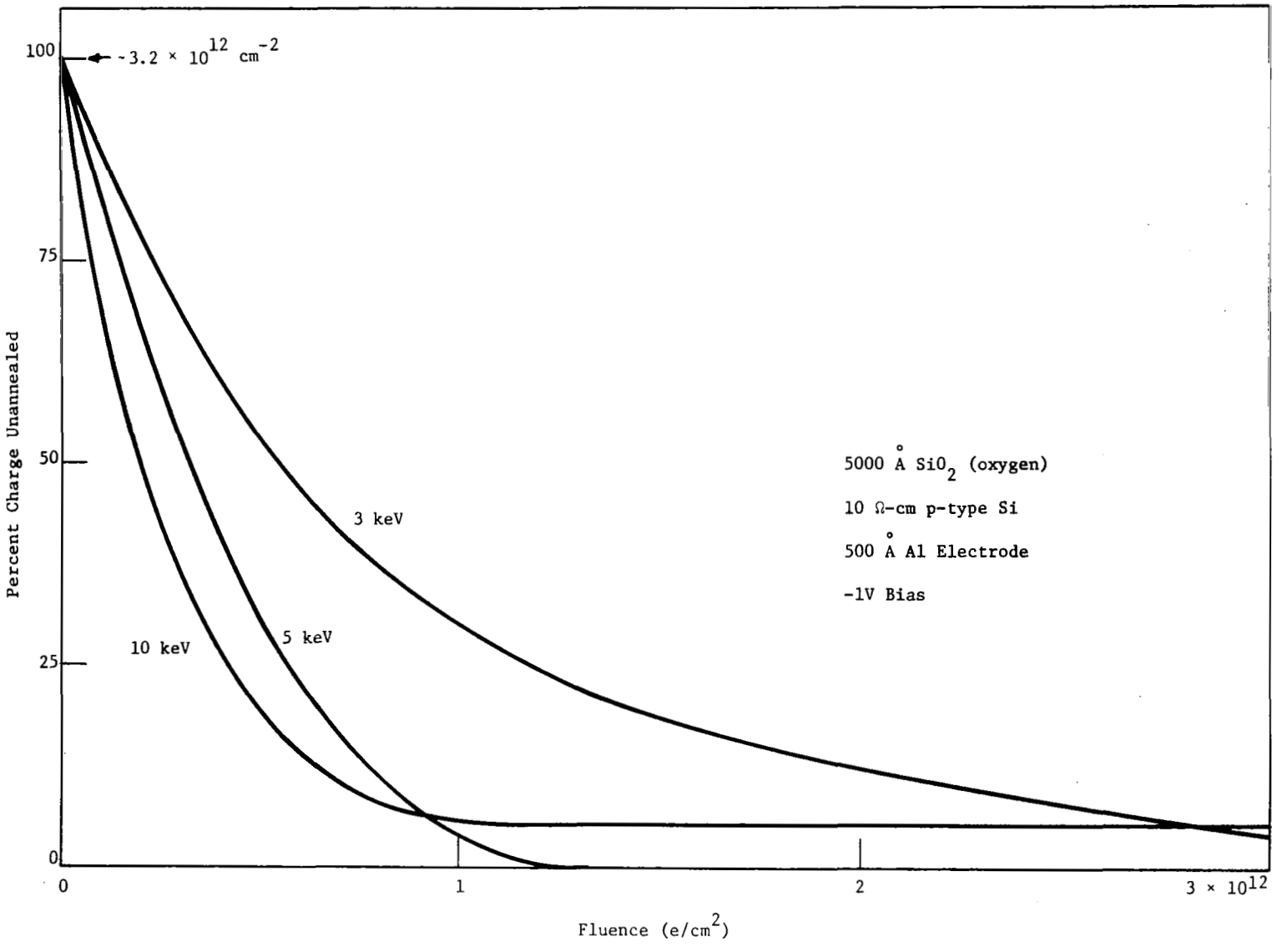

Figure 23. Radiation Annealing of Positive Space Charge in 5000 Å Sample

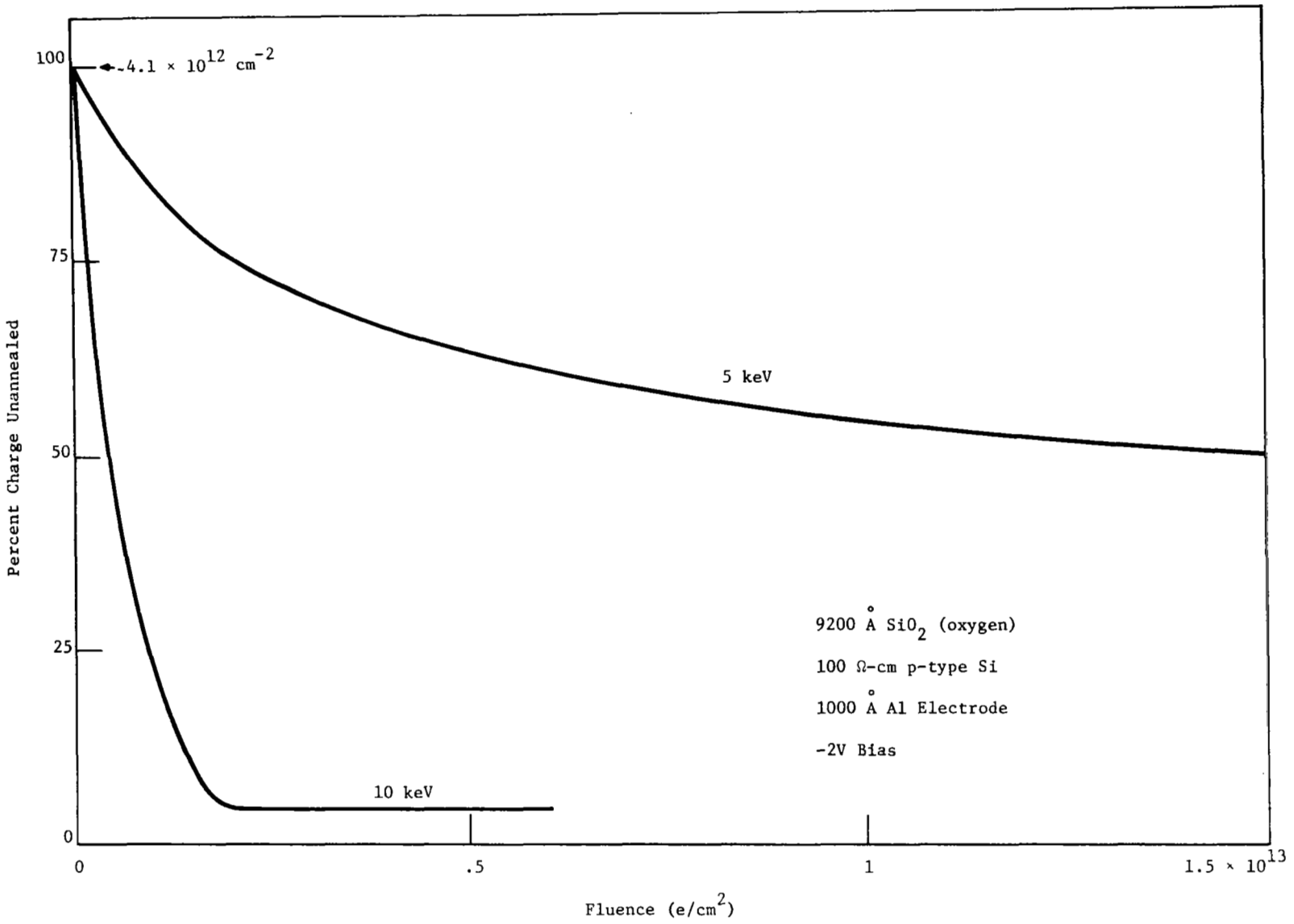

Figure 24. Radiation Annealing of Positive Space Charge in 9200 Å Sample

silicon dioxide has been reported by Williams to be 4.25 eV (Ref. 25), it is likely that electrons injected from the silicon are recombining with the trapped positive charge and unlikely that the trapped charge is being activated. Failure to observe annealing at 4.25 eV in this experiment can be attributed to the low intensity of monochromatic light coupled with a low photon capture cross section near this threshold. It was also noted that for a given exposure more charge was annealed at zero sample bias than at large positive or negative biases. This lends support to the theory of electron injection and subsequent recombination, since a field in one direction should reduce electron injection across the barrier while a strong field in the other direction would increase the electrons drift velocity through the oxide thereby reducing the time available for recombination in the space charge region. An applied field should not significantly affect an activation process, although it could have an influence on retrapping of activated carriers.

Failure to activate the trapped charge at energies below the photoemission threshold for electrons indicates that the trapping levels are either deeper than 4.25 eV or have such a small photon capture cross section that a much higher incident light intensity is required to effect a noticeable charge reduction.

Thermal Annealing

All of the positive charge induced in SiO_2 by low energy electron irradiation can usually be completely removed by annealing at 300°C for about 10 minutes in an inert environment. Following an initial 300°C anneal, samples could be irradiated and annealed repeatedly without showing any appreciable change in the charge build-up characteristics.

The charge induced in samples irradiated at 200 keV and 1 MeV was considerably more difficult to remove. From 30 to 60 minutes at 300°C was required to completely anneal these units. The introduction of deeper trapping levels associated with localized defects produced in the oxide by the high energy electrons affords a possible explanation for this increased difficulty in annealing.

Isochronal annealing of samples irradiated at both high and low energies was performed to obtain an activation energy for the trapped charge. Here, an irradiated sample was subjected to temperatures from 50°C to 300°C in 25°C steps. After 10 minutes at each temperature the sample was rapidly cooled to room temperature where a C-V measurement was made. No dc bias was applied to the sample while at elevated temperature to prevent any C-V shift resulting from the drift of ionic impurities in the oxide.

The results of two isochronal anneals made on the same sample are shown in Fig. 25. The logarithm of the percent charge annealed in the oxide as determined from the C-V measurements is plotted against 1/T.

This particular sample had a 2,500 Å oxygen oxide and was irradiated both times at 10 keV with +2V applied bias. The disparity between curves is typical of the data spread observed for both steam and oxygen samples irradiated at high and low energies. The non-linearity of the curves indicates either that the trapping levels are distributed in energy or that this is not an activated process. The slopes of straight lines fitted to linear portions of the curves yielded activation energies ranging from 0.28 to 0.46 eV. Since the room temperature stability of the trapped positive charge requires much deeper trapping levels, this annealing data infers that a process more complex than simple activation of the trapped charge is involved.

Charge release was also observed as a function of time in several samples annealed at constant temperatures. At room temperature the annealed charge was found almost invariably to be a linear function of the logarithm of the elapsed time out to 10^5 seconds or more. At elevated temperatures this linearity was less pronounced but was frequently observed over a shorter time interval. Figure 26 shows annealing curves for a 2,500 Å steam oxide annealed at three different temperatures. The initial portions of the 100°C and 200°C curves are distorted as a result of both the finite time required to reach the annealing temperature and the temperature dependence of charged states at the $Si-SiO_2$ interface.

Linearity of released or annealed charge with ln t can be explained by several models. One such model is based on the Schottky-Richardson effect, whereby electrons are thermally emitted from the silicon across the $Si-SiO_2$ barrier into the oxide where they recombine with the trapped charge. The barrier is attenuated by the electric field produced at the interface by the trapped positive charge. The band diagram for the $Si-SiO_2$ system before and after introduction of the positive space charge into the oxide is sketched in Fig. 27. The barrier, ϕ, is reduced by $\Delta\phi$, which from the Schottky effect is

$$\frac{q\Delta\phi}{kT} = \frac{1}{2kT}\left[\frac{q^3}{\pi\varepsilon}\right]^{1/2} E^{1/2} = \beta E^{1/2} , \qquad (12)$$

where E is the electric field at the interface. The electron current density flowing across the barrier into the oxide is given by the Schottky-Richardson equation:

$$J_n = \frac{dQ_n}{dt} = C_1 T^2 \exp\left[\frac{-q\phi}{kT} + \beta E^{1/2}\right] , \qquad (13)$$

which can be reduced to

$$\frac{dQ_n}{dt} = C_2(T)\, e^{\beta E^{1/2}} . \qquad (14)$$

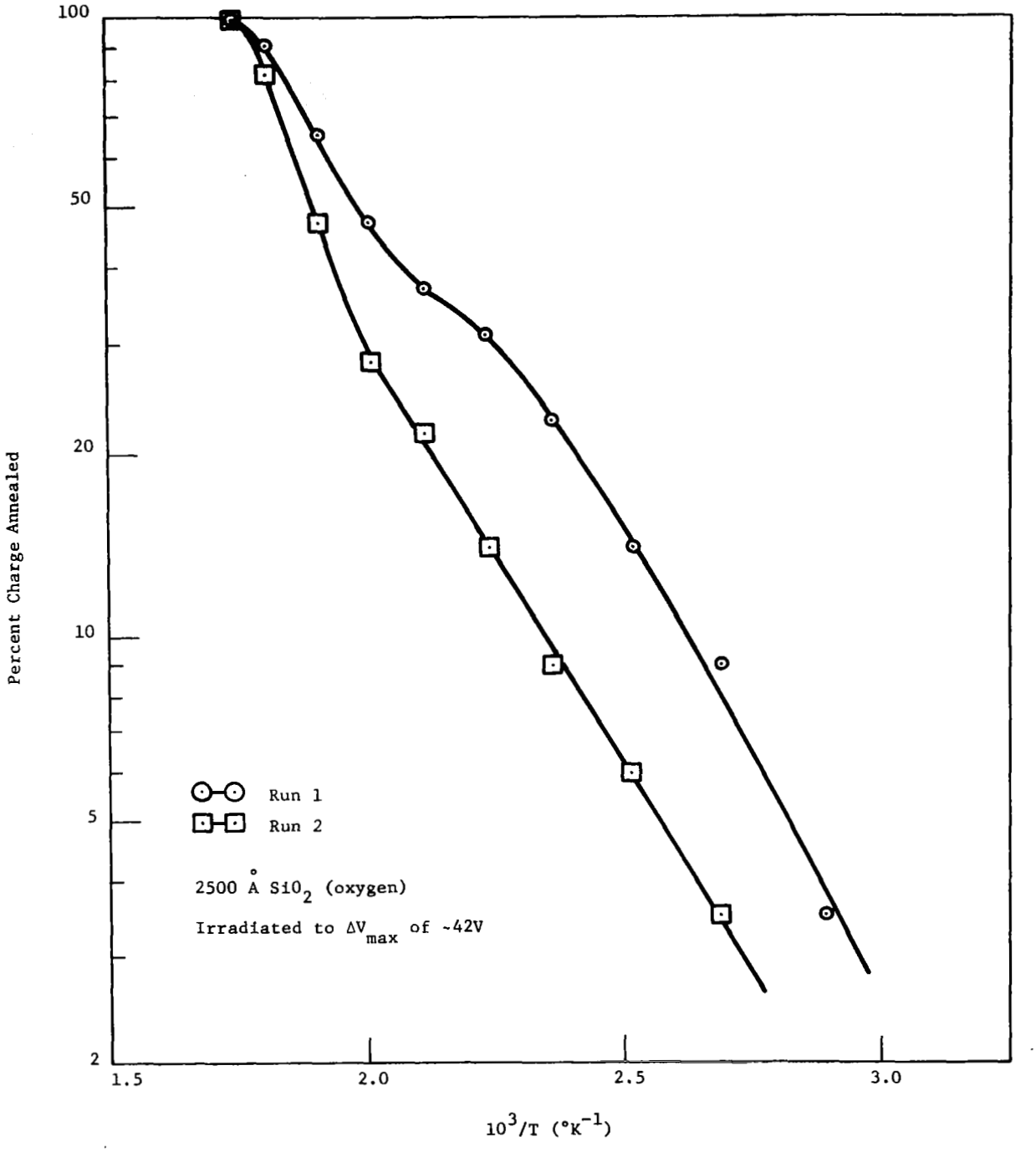

Figure 25. Isochronal Annealing Curves for Irradiated MOS Structure

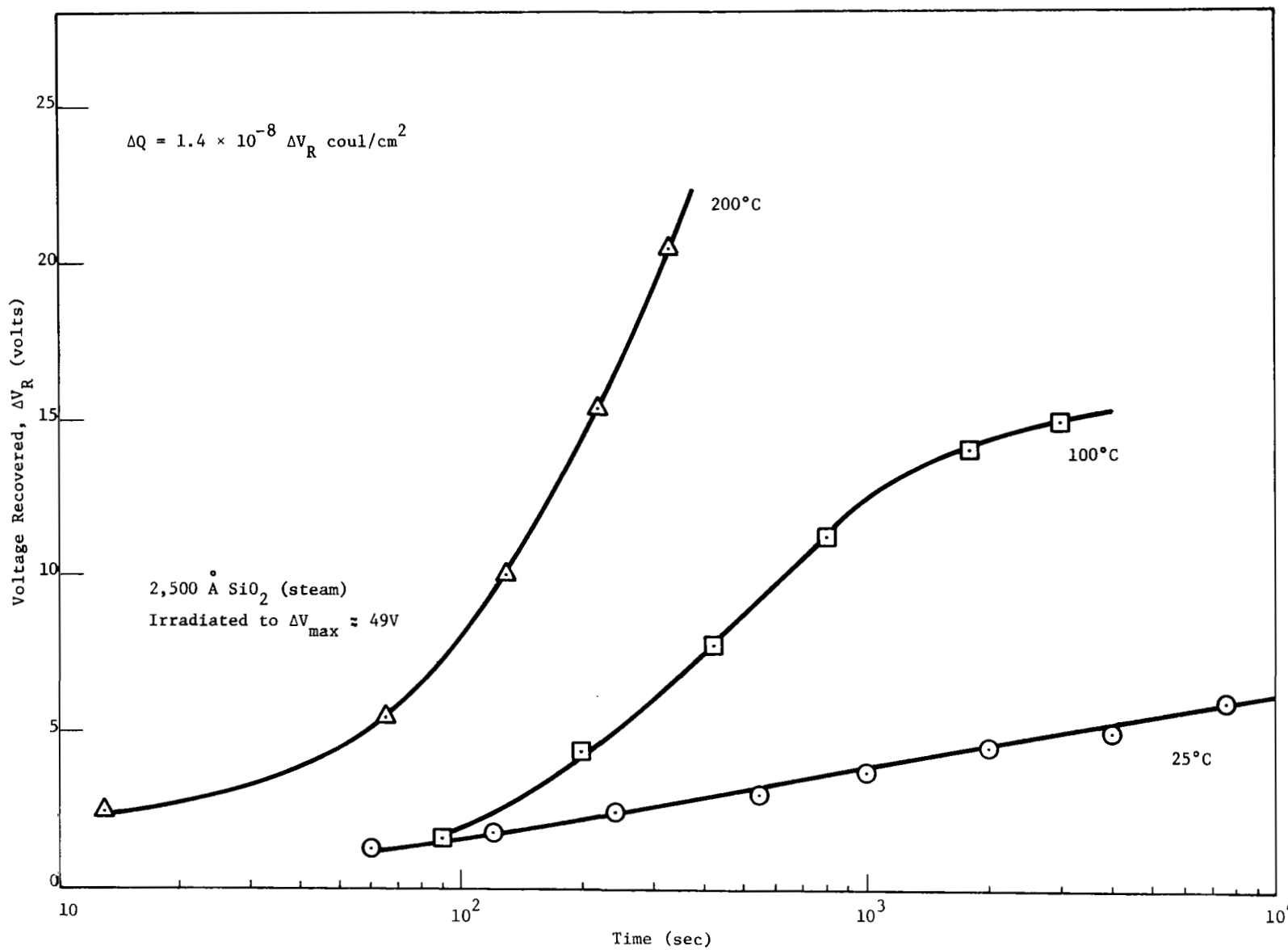

Figure 26. Constant Temperature Anneal of Positive Space Charge in SiO_2

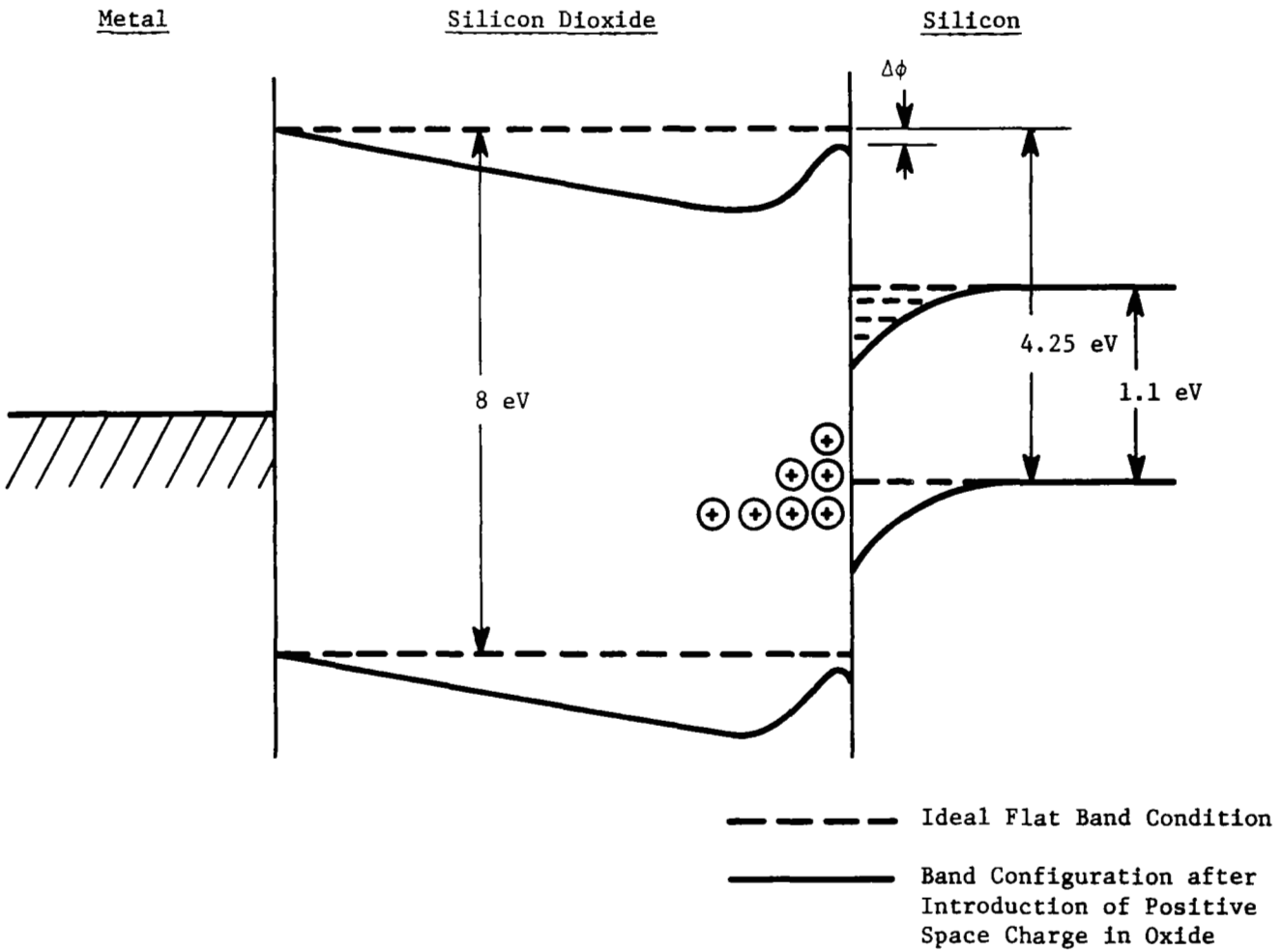

Figure 27. Simplified Band Diagram for $Si-SiO_2$ System

If the initial positive charge, Q_p, is trapped in the oxide near the silicon interface such that the space charge region is much narrower than the total oxide thickness, then the field can be written

$$E = \frac{Q_p - Q_n}{\varepsilon} = E_o - Q_n/\varepsilon \tag{15}$$

and

$$E^{1/2} \approx E_o^{1/2} \left(1 - \frac{Q_n}{2\varepsilon E_o}\right) . \tag{16}$$

Inserting this value of $E^{1/2}$ into Eq. (14), and solving for Q_n using the boundary condition that $Q_n = 0$ at $t = 0$, one obtains

$$Q_n = \frac{1}{C_4} \ln [C_3 C_4 t + 1] \tag{17}$$

where

$$C_3 = C_2(T)\, e^{\beta E_o^{1/2}} \tag{18}$$

and

$$C_4 = \frac{\beta}{2\varepsilon E_o^{1/2}} . \tag{19}$$

For $t >> 1/C_3C_4$, Eq. (17) can be written

$$Q_n \approx \frac{1}{C_4} \ln C_3 C_4 + \frac{1}{C_4} \ln t . \tag{20}$$

If all of the injected charge Q_n recombines with the trapped positive charge, then Eq. (20) expresses the annealed or "released" charge as a function of time. According to Eq. (20), Q_n is linear function of ln t with a slope of $1/C_4$. From Eqs. (12), (15) and (19), the annealing slope becomes

$$m = 4\varepsilon \frac{kT}{q} \left(\frac{\pi Q_p}{q}\right)^{1/2} . \tag{21}$$

As Q_n increased toward εE_o, Eq. (16) is no longer valid; the annealing curve departs from its linear dependence and Q_n asymptotically approaches Q_p.

The 2,500 Å sample whose annealing curves are shown in Fig. 26 was irradiated to a Q_p of about 6.9×10^{-7} coul/cm^2 prior to each anneal. The slopes calculated from Eq. (21) range from 1.0×10^{-7} coul/cm^2 at 25°C to 1.6×10^{-7} coul/cm^2 at 200°C. The slopes measured over linear portions of the curves in Fig. 26 extend from approximately 1.5×10^{-8} at 25°C to 1.5×10^{-7} at 200°C. The observed dependence of annealing slope on absolute temperature is much greater than that predicted by Eq. (21) and thus is not consistent with a simple Schottky-Richardson effect. Also, using this model ϕ and $\Delta\phi$ were calculated to be about 1.4 and 0.3 eV, respectively. This value for ϕ is in sharp contrast to the previously reported Si-SiO_2 barrier of 4.25 eV.

A linear dependence of released charge on ln t can also be explained by assuming thermal activation of trapped carriers from traps uniformly distributed in energy. Such a dependence has been shown to exist in the case of electrons thermally released from traps uniformly distributed in the forbidden band of a dielectric (Ref. 12). However, in this process the annealing slope should again be a linear function of absolute temperature.

In summary, it appears from the available data that thermal annealing of the positive space charge in SiO_2 is a complex process or combination of processes which may or may not include those discussed above. Electron tunneling from silicon into states in the oxide is also a possibility. Further efforts are needed to develop a satisfactory model for charge annealing.

External Charge Transfer

No significant external charge transfer was observed from irradiated SiO_2 structures either at room temperature or during high temperature anneals. Indeed, none would be expected from an irradiated structure in which the space charge is trapped adjacent to an interface. This result is in contrast to measurements made following electron irradiation of evaporated SiO samples, in which appreciable external charge transfer was observed (Ref. 11). This charge transfer has been attributed to the thermal release of spatially trapped electrons introduced during irradiation. The same results were obtained during this work upon irradiation of 3.5μ SiO samples with non-penetrating electrons. As pointed out earlier, attempts to make C-V measurements on the evaporated oxide structures were not successful, therefore this technique could not be used to verify the radiation-induced negative charge build-up inferred from the charge release measurements.

SECTION V

RADIATION EFFECTS ON MOS DEVICES

The results of the preceeding work on charge build-up and release in silicon dioxide are directly applicable to the performance of MOS field-effect transistors (MOSFETs) in a radiation environment. The channel or drain current for the linear MOSFET structure, shown in Fig. 28, is given by (Ref. 26)

$$I_D = \frac{\bar{\mu}_n C_o}{L^2} [(V_g - V_t) V_D - V_D^2/2] , \qquad (22)$$

where $\bar{\mu}_n$ is the average surface mobility of electrons in the channel and V_t is the gate voltage required to induce an inversion layer in the channel between source and drain. This threshold voltage is defined by

$$V_t = - \frac{Q_t}{C_o} , \qquad (23)$$

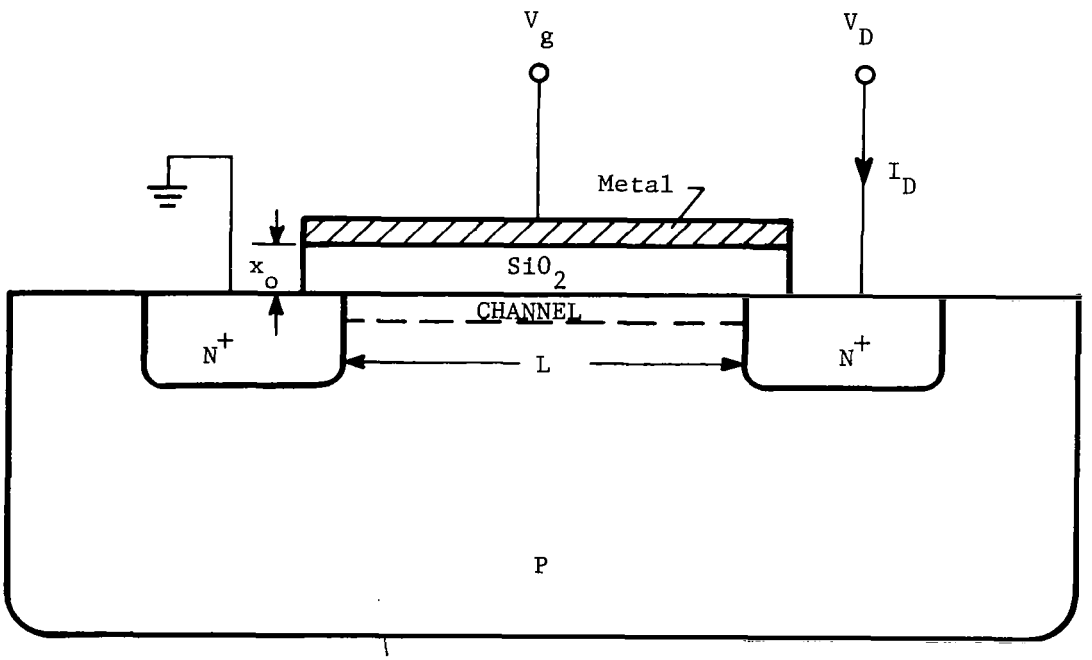

Figure 28. Linear MOSFET Structure

where Q_t is the total surface charge density reflected at the interface as a result of bulk oxide charge and charged interface states. Equation (22) only holds for the gradual channel approximation where V_D is not large enough to pinch off the channel at the drain. From Eqs. (22) and (23) it is apparent that the drain current is directly affected by any change in oxide charge. The drain current deviation resulting from a charge variation ΔQ_t is given by

$$\Delta I_D = -\frac{\bar{\mu}_n \epsilon_{ox} V_D}{L^2 d} \Delta V_t = \frac{\bar{\mu}_n V_D}{L^2} \Delta Q_t \ . \qquad (24)$$

Thus the radiation-induced positive charge in SiO_2 will produce a parallel shift in the conductance characteristics of the MOSFET toward more negative gate voltages as indicated in Fig. 29 for both n-channel and p-channel devices. The data in Sec. II can be used to approximate the voltage shift produced in a MOSFET at a particular electron fluence and gate bias provided the gate oxide thickness is known. In addition to the parallel shift of conductance characteristics, the slope of these curves can deteriorate with increasing exposure much in the same manner as does the slope of the C-V characteristic. This slope or transconductance g_m is seen from Eq. (22) to be

$$g_m = \left.\frac{\partial I_D}{\partial V_g}\right|_{V_D} = \frac{\bar{\mu}_n C_o V_D}{L^2} \ . \qquad (25)$$

The channel mobility is less than that of the bulk due to surface scattering of carriers and is affected by the charge present at the interface. If there are any fast interface states, $\bar{\mu}_n$ will also become a function of the surface potential.

As in the case of the simple MOS structure, it should be possible to minimize charge build-up and the resulting shift in conductance characteristics by the application of a small negative bias to the gate electrode during exposure. Radiation damage to a MOSFET will for all practical purposes be permanent at room temperature, but recovery should be possible in most devices by annealing at 300°C provided, of course, the device can withstand such an environment. Again, devices employing steam-grown oxides should be more tolerant to radiation than those with oxides grown in oxygen.

The effects produced by low energy charged-particle radiation on an off-the-shelf MOSFET device will be moderated by attenuation in the surrounding encapsulation. If the mass-thickness of the intervening material is known, the incident radiation damage threshold can be calculated for a given unit.

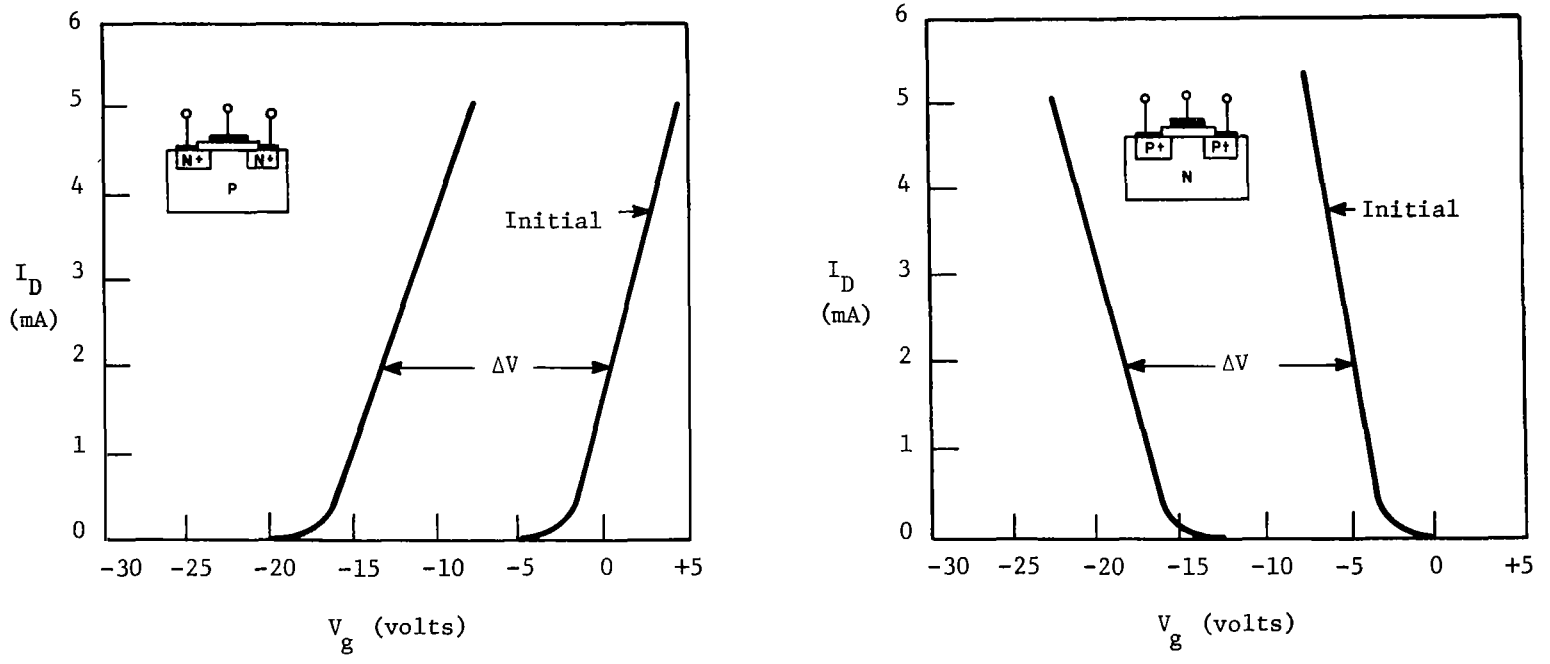

Figure 29. Typical Radiation Induced Shifts in Conductance Characteristics of N- and P-Channel MOSFETs

At higher particle energies, it becomes more difficult to predict how a particular device will be affected because of the various channel characteristics which come into play. For example, in the case of p-channel MOSFETs irradiated with 1.5 MeV electrons, the gate threshold voltage has been reported to increase rapidly with fluence toward a more negative voltage and then decrease and saturate at some less negative voltage level (Ref. 27). Since the threshold voltage was determined by measuring the gate voltage needed to produce a particular channel current rather than by directly measuring the voltage required to produce inversion of the surface layer, both oxide charge and channel mobility variations become suspect. Certainly effects on $\bar{\mu}_n$ become even more pronounced at energies sufficiently penetrating to produce damage in the channel itself.

Net positive voltage shifts in transfer characteristics have been reported for n-channel devices irradiated with 125 keV and 1 MeV electrons, Co^{60} gammas, and 16.8 MeV protons (Ref. 28). Also, the transfer characteristics were found to be unstable following the electron and gamma irradiations. The positive shift has been attributed to negative charge trapped in the oxide and the instability to the presence of surface trapping sites which can exchange charge with the silicon. Unfortunately C-V measurements were not made to verify the negative space charge in the oxide. However, the gate oxides of the devices tested consisted of thermally grown SiO_2 plus chemically deposited, phosphorus-doped oxide. The deposited oxide, like evaporated SiO, might be responsible for a negative oxide charge.

In summary, radiation effects on channel mobility in MOS devices must be considered, particularly at high energies; however, it would appear that the predominant radiation effect in these devices is the oxide space charge build-up, which at least for thermally grown oxides displays certain consistent features as summarized in the following section.

SECTION VI

CONCLUSIONS AND RECOMMENDATIONS

A number of characteristics of radiation-induced space charge build-up and release have become apparent during this work and are consistent with results reported by other investigators. These characteristics are summarized below:

(1) A semi-permanent, positive charge density is induced in silicon dioxide upon exposure to the various types of ionizing radiation.

(2) The charge build-up in an MOS structure is strongly dependent on the bias applied during irradiation. The silicon image charge is much larger when the electrode polarity during exposure is positive. Some charge accumulates at zero bias, but the smallest image charge is induced at small negative biases.

(3) Both the saturated and unsaturated induced charge densities have been observed to exhibit a linear to parabolic dependence on applied bias.

(4) Space charge build-up is a function of the energy absorbed by the oxide, particularly that absorbed near the oxide-silicon interface.

(5) The induced charge shows little, if any, dependence on the flux density.

(6) The radiation sensitivity of a particular oxide is strongly influenced by the method of oxidation and by the previous thermal history of the oxide. Steam-grown oxides are generally less sensitive to radiation than are oxides prepared in oxygen. Samples annealed at or near 300°C show less charge build-up upon irradiation than do unannealed samples.

(7) Irradiation, annealing, and etching experiments together with most of the models proposed for space charge formation indicate that during irradiation at positive bias most of the oxide charge is trapped at or near the oxide-silicon interface.

(8) The positive space charge can be annealed optically, thermally, and by irradiation at small negative bias levels. The annealing process appears to result in each case from recombination of trapped positive charge with electrons injected into the oxide.

Although a completely satisfactory quantitative model for space charge formation in the irradiated MOS structure has yet to be developed, a basic understanding of radiation effects in thermally-grown SiO_2 is beginning to

emerge. Recently, deposited oxides, oxides passivated with phosphorus, and silicon nitride have been studied for possible device applications. Although stability problems remain to be overcome in silicon nitride, it has been found to be more radiation resistant than SiO_2. Radiation studies on deposited oxide layers have pointed toward a possible negative space charge build-up in some of these films. Whether phosphorus passivation has any effect on the radiation sensitivity of SiO_2 is still questionable.

Since a suitable substitute for SiO_2 in silicon devices and integrated circuits has not been found and seems unlikely in the immediate future, it is recommended that investigations of the effects of various types of ionizing radiation on SiO_2 continue. Of particular interest are oxides having contamination levels in the range from 10^{10} to 10^{11} cm^{-2}, oxides passified with phosphorus, and combinations of thermally-grown and deposited oxide layers with and without phosphorus passivation. A particular combination of oxide layers might minimize the net space charge through compensating positive and negative charge regions. Multiple oxide layers might also cause the charge to be trapped near an interior interface and away from the oxide-silicon interface, such that it will have a smaller influence on the underlying silicon surface.

The predominant radiation effect on MOSFET devices appears to result from the oxide charge build-up, although changes in channel characteristics can be significant under certain conditions. Testing of selected devices in various radiation environments is recommended to isolate and identify the effects on device characteristics resulting from changes in both oxide and channel parameters.

Efforts to solve the two-carrier model should continue in order to obtain a complete understanding of space charge formation in the MOS structure. A knowledge of how the individual oxide properties affect the magnitude, distribution, and polarity of this space charge should expedite the development of more radiation resistant oxides and other dielectric materials.

APPENDIX

FORMULATION OF TWO CARRIER MODEL FOR SPACE CHARGE BUILD-UP

Derivation of Trapping and Transport Equations

The basic processes of carrier generation, trapping, and recombination through electron and hole traps located at energy levels E_{tn} below the conduction band and E_{tp} above the valence band, respectively, are shown in Fig. A-1 for the conventional energy band configuration. Using the symbols defined in the table, the emission and capture rates can be written as follows:

$$
\begin{aligned}
r_1 &= c_{nt} n\ (N_{tn} - n_t) \\
r_2 &= s_n n_t\ \exp(-E_{tn}/kt) \\
r_3 &= s_p p_t\ \exp(-E_{tp}/kt) \\
r_4 &= c_{pt} p\ (N_{tp} - p_t) \\
r_5 &= c_{nr} n p_t \\
r_6 &= c_{pr} p n_t \\
r_7 &= c_1 N_c\ (N_{tp} - p_t) \\
r_8 &= c_2 N_v\ (N_{tn} - n_t)
\end{aligned}
\qquad \text{(A-1)}
$$

If g_n and g_p are the generation rates of excess carriers, then the continuity equations for free electrons and holes are

$$
\begin{aligned}
\frac{\partial n}{\partial t} = &- c_{nt} n(N_{tn} - n_t) + s_n n_t \exp(-E_{tn}/kt) \\
&- c_{nr} n p_t + c_1 N_c (N_{tp} - p_t) + g_n + \frac{1}{q}\frac{\partial J_n}{\partial x}
\end{aligned}
\qquad \text{(A-2)}
$$

$$
\begin{aligned}
\frac{\partial p}{\partial t} = &- c_{pt} p(N_{tp} - p_t) + s_p p_t \exp(-E_{tp}/kt) \\
&- c_{pr} p n_t + c_2 N_v (N_{tn} - N_t) + g_p - \frac{1}{q}\frac{\partial J_p}{\partial x} \quad .
\end{aligned}
\qquad \text{(A-3)}
$$

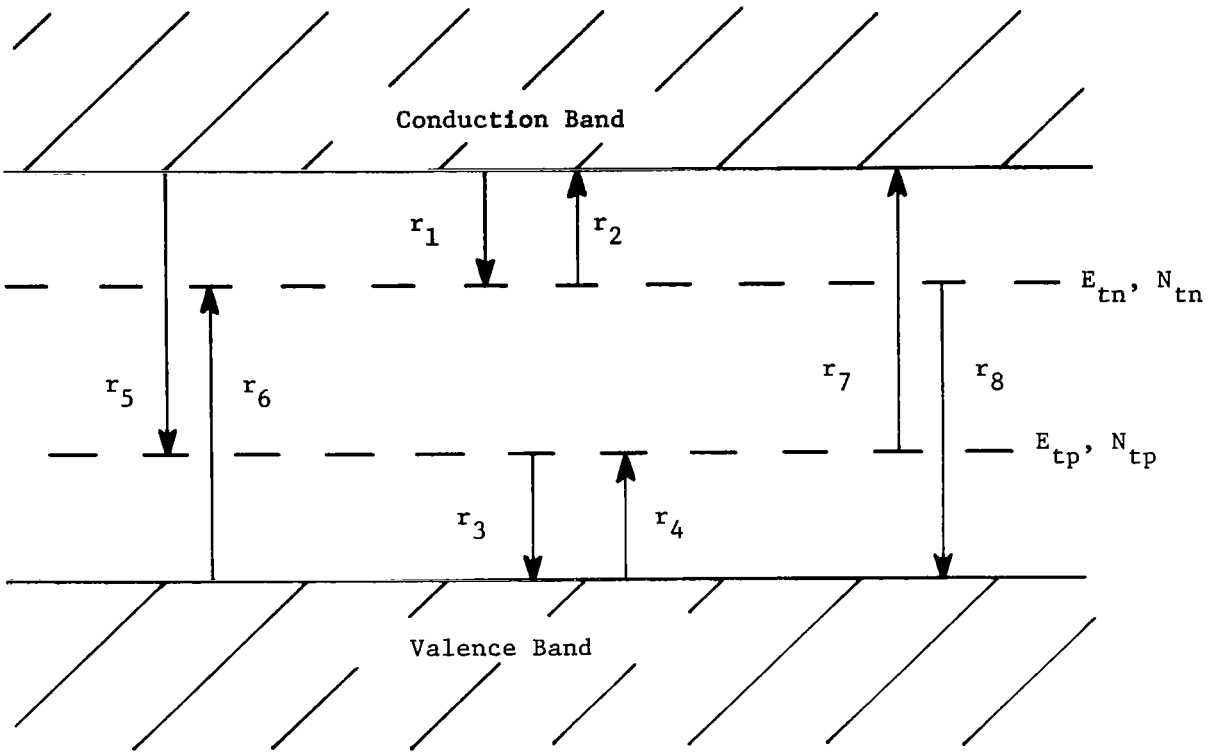

Figure A-1. Generation, Trapping, and Recombination Processes for Electron and Hole Traps

The net rates of change of trapped carriers are

$$\frac{\partial n_t}{\partial t} = c_{nt} n(N_{tn} - n_t) - s_n n_t \exp(-E_{tn}/kt) - c_{pr} p n_t + c_2 N_v (N_{tn} - n_t) \quad \text{(A-4)}$$

$$\frac{\partial p_t}{\partial t} = c_{pt} p(N_{tp} - p_t) - s_p p_t \exp(-E_{tp}/kt) - c_{nr} n p_t + c_1 N_c (N_{tp} - p_t) \; . \quad \text{(A-5)}$$

Table of Symbols

C_1, C_2 - release rate constants

c_{nt} - electron capture coefficient for electron trap

c_{nr} - electron capture or recombination coefficient for hole trap

c_{pt} - hole capture coefficient for hole trap

c_{pr} - hole capture or recombination coefficient for electron trap

J_n - electron current density

J_p - hole current density

n - free electron density

n_t - trapped electron density

N_c - effective density of states in conduction band

N_V - effective density of states in valence band

N_{tn} - electron trap density

N_{tp} - hole trap density

p - free hole density

p_t - trapped hole density

r - emission or capture rate ($cm^{-3}sec^{-1}$)

s_n - electron attempt to escape frequency (sec^{-1})

s_p - hole attempt to escape frequency (sec^{-1})

μ_n - electron mobility (cm^2/volt sec)

μ_p - hole mobility (cm^2/volt sec)

In the case of electron irradiation, the generation rates can be written

$$g_n = (1 + \gamma)g \text{ and } g_p = \gamma g \ , \qquad \text{(A-6)}$$

where g is the generation rate of incident electrons and γ is the average number of electron-hole pairs created by each incident electron. In general, γ is a function of both x and g.

Release of trapped carriers can be neglected during charge build-up since the times under consideration are relatively short compared with observed release times. Rate equations (A-2) through (A-5) are then reduced to

$$\frac{\partial n}{\partial t} = - c_{nt} n(N_{tn} - n_t) - c_{nr} n p_t + g_n + \frac{1}{q} \frac{\partial J_n}{\partial x} \qquad \text{(A-7)}$$

$$\frac{\partial p}{\partial t} = - c_{pt} p(N_{tp} - p_t) - c_{pr} p n_t + g_p - \frac{1}{q} \frac{\partial J_p}{\partial x} \qquad \text{(A-8)}$$

$$\frac{\partial n_t}{\partial t} = c_{nt} n(N_{tn} - n_t) - c_{pr} p n_t \qquad \text{(A-9)}$$

$$\frac{\partial p_t}{\partial t} = c_{pt} p(N_{tp} - p_t) - c_{nr} n p_t \ . \qquad \text{(A-10)}$$

These reduced equations include capture of free carriers by traps and recombination of trapped carriers with free carriers of the opposite type.

Electron trapping can be neglected in SiO_2 since $\mu_n \tau_n E$ is usually greater than the oxide thickness even for small applied fields. Also, no electron trapping has been observed during radiation recovery experiments; therefore, it seems safe to assume that $N_{tn} = 0$. If both the applied field and the generation rate are constant, then after an initial transient the free carrier concentrations will approach a steady state condition. Thus, the rate equations are finally reduced to

$$\frac{\partial p_t}{\partial t} = c_{pt} p(N_{tp} - p_t) - c_{nr} n p_t \qquad \text{(A-10)}$$

$$\frac{\partial n}{\partial t} = - c_{nr} n p_t + g_n + \frac{1}{q} \frac{\partial J_n}{\partial x} \approx 0 \qquad \text{(A-11)}$$

$$\frac{\partial p}{\partial t} = - c_{pt} p (N_{tp} - p_t) + g_p - \frac{1}{q} \frac{\partial J_p}{\partial x} \approx 0 \ . \qquad \text{(A-12)}$$

Neglecting carrier diffusion and assuming that $p-n << p_t$, the current equations and Poisson's equation can be written

$$J_n = q\mu_n nE \qquad \text{(A-13)}$$

$$J_p = q\mu_p pE \qquad \text{(A-14)}$$

$$\frac{\partial E}{\partial x} = \frac{q}{\varepsilon} p_t \ . \qquad \text{(A-15)}$$

Equations (A-10) through (A-15), together with the appropriate boundary conditions, describe the oxide during irradiation. These equations must be solved numerically to obtain the free and trapped carrier densities as a function of time and position within the oxide.

Computer Solution

To numerically solve Eqs. (A-10) through (A-15), it becomes convenient to rewrite them in terms of normalized variables. After combining Eqs. (A-13) and)A-14) with (A-11) and (A-12), respectively, the four normalized equations are:

$$\frac{\partial \bar{p}_t}{\partial \bar{t}} = \bar{p} \ (1 - \bar{p}_t) - \gamma \bar{n} \bar{p}_t \qquad \text{(A-16)}$$

$$\frac{\partial \bar{n}}{\partial \bar{x}} = - \frac{(\bar{\mu}_n - 1)\bar{n}\bar{p}_t + G_n}{\bar{\mu}_n F} \qquad \text{(A-17)}$$

$$\frac{\partial \bar{p}}{\partial \bar{x}} = - \frac{(\bar{\mu}_p - 1)\bar{p}\bar{p}_t + \bar{p} - G_p}{\bar{\mu}_p F} \qquad \text{(A-18)}$$

$$\frac{\partial F}{\partial \bar{x}} = \bar{p}_t \ , \qquad \text{(A-19)}$$

where

$$\bar{x} = \frac{x}{x_o} \qquad \gamma = \frac{c_{nr}}{c_{pt}}$$

$$\bar{p}_t = \frac{p_t}{N_{tp}} \qquad \bar{t} = \frac{t}{\tau_{pt}}$$

$$\bar{n} = \frac{n}{N_{tp}} \qquad \bar{p} = \frac{p}{N_{tp}}$$

$$\bar{\mu}_p = \frac{q\mu_p}{\varepsilon c_{pt}} \qquad \bar{\mu}_n = \frac{q\mu_n}{\varepsilon c_{nr}}$$

$$G_p = \frac{g_p}{c_{pt} N_{tp}^2} \qquad G_n = \frac{g_n}{c_{nr} N_{tp}^2}$$

$$F = \frac{\varepsilon E}{q N_{tp} x_o} \qquad x_o = \text{dielectric thickness} .$$

Equation (A-19) is integrated to obtain an expression for F as a function of $\bar{x}$ subject to the boundary conditions on v(0) and $v(x_o)$. If it is assumed that there is no trapped charge initially, then upon integrating Eq. (A-19) one obtains

$$F(\bar{x}) = - V_{app} - \int_o^1 \left[\iint_o^{x'} \bar{p}_t dx'' \right] dx' + \int_o^{\bar{x}} p_t dx' , \qquad \text{(A-20)}$$

where V_{app} is the magnitude of the applied voltage. Equations (A-16), (A-17), (A-18), and (A-20) are in a form convenient for numerical solution of the four unknowns $\bar{p}_t$, $\bar{n}$, $\bar{p}$, and F as a function of time and position within the dielectric. After selecting appropriate values for the various constants, the following procedure was followed in solving these four equations:

(1) Assume that $\bar{p}_t$ is known initially (here $\bar{p}_t = 0$ at $\bar{t} = 0$).

(2) Solve Eq. (A-20) for the field F(x).

(3) Solve Eqs. (A-17) and (A-18) for $\bar{n}(x)$ and $\bar{p}(x)$ at the initial time using the boundary conditions that $\bar{n}(x) = 0$ at one boundary and $\bar{p}(x) = 0$ at the other. This assumes that $F \neq 0$ anywhere within the sample and that there is no carrier injection into the oxide at the boundaries.

(4) Using $F(x)$, $\bar{n}(x)$, and $\bar{p}(x)$ calculate $\frac{\partial \bar{p}_t}{\partial \bar{t}}$, then extrapolate to find $\bar{p}_t$ at the next time interval.

(5) Repeat the above steps using the new $\bar{p}_t$.

The integrations on $\bar{x}$ and $\bar{t}$ were done by a predictor-corrector method with the solutions iterated until consistent values were obtained at each point in time.

The computer solutions followed the expected results during the initial intervals of charge build-up. In the region near one interface ($\bar{x} = 1$) the concentration of free holes ($\bar{p}$) began to increase while the free electron concentration ($\bar{n}$) became smaller as the induced carriers were swept in opposite directions by the applied field. The concentration of trapped holes ($\bar{p}_t$) also began to build-up, generally following the free hole distribution between the two boundaries. As $\bar{p}_t$ grew larger, the field F increased in the space charge region and became smaller near the other interface ($\bar{x} = 0$). Finally, at this interface F approached zero, $\bar{n}$ became unbounded, and the solution broke down. At this point it became apparent that a diffusion term must be included in Eq. (A-13) to prevent a build-up of free electrons in the region of the zero field point. Unfortunately, this added term complicates the problem making a numerical solution more difficult. The difficulties encountered in developing a program to solve the resulting equations were not overcome during this project.

REFERENCES

1. Linder, R.: Semiconductor Surface Varactor. BSTJ, May 1962, p. 803.

2. Grove, A. S.; Deal, B. E.; Snow, E. H.; and Sah, C. T.: Investigation of Thermally Oxidized Silicon Surfaces using Metal-Oxide-Semiconductor Structures. Solid-State Electronics, Pergamon Press, Vol. 8, 1965, p. 145.

3. Hofstein, S. R.; and Warfield, G.: Physical Limitations on the Frequency Response of a Semiconductor Surface Inversion Layer. Solid-State Electronics, Pergamon Press, Vol. 8, 1965, pp. 321-41.

4. Goetzberger, A.: Ideal MOS Curves for Silicon. BSTJ, Sept. 1966, p. 1097.

5. Sah, C. T.: Theory of the Metal Oxide Semiconductor Capacitor. Solid State Electronics Lab., TR No. 1, Univ. of Illinois, Urbana, Ill., Dec. 1964.

6. Burger, R. M.; and Donovan, R. P.: "Fundamentals of Silicon Integrated Device Technology, Vol. I, Oxidation, Diffusion, and Epitaxy", Englewood Cliffs, N. J., Prentice-Hall, Inc., 1967.

7. Deal, B. E.; Sklar, M.; Grove, A. S.; and Snow, E. H.: Characteristics of the Surface State Charge of Thermally Oxidized Silicon. J. Electrochem. Soc., Vol. 114, No. 3, March 1967, p. 266.

8. Fewer, D. R.; and Carlson, H. G.: Report on Surface Studies. Tex. Instr. RADC-TR-66-776, March 1967.

9. Schmidt, R.: "Alkali Contamination of SiO_2 Surfaces of Planar Silicon Semiconductor Devices During Deposition of Metal Layers of Evaporation", Paper delivered at Electrochem. Soc. Meeting, Dallas, Tex., 1967.

10. Buck, T. M.; Allen, F. G.; Dalton, J. V.; and Struthers, J. D.: Studies of Sodium in SiO_2 Films by Neutron Activation and Radiotracer Techniques. J. Electrochem. Soc., Vol. 114, 1967, p. 862.

11. Monteith, L. K.; Hauser, J. R.; and Royal, T. M.: Charge Storage Effects in Mylar Resulting from Electron Irradiation. NASA CR-656, 1966.

12. Monteith, L. K.: Study on the Electronic Irradiation Effects on Capacitor-Type Micrometeoroid Detectors. NASA CR-312, 1965.

13. Kanter, H. S.: Contribution of Backscattered Electronics to Secondary Electron Formation. Phys. Rev., Vol. 121, No. 3, Feb. 1961, p. 681.

14. Zaininger, K. H.: Irradiation of MIS Capacitors with High Energy Electrons. IEEE Trans. Nucl. Sci., NS-13, Dec. 1966, p. 237.

15. Grove, A. S.; and Snow, E. H.: A Model for Radiation Damage in Metal-Oxide-Semiconductor Structures. Proc. IEEE, June 1966, p. 894.

16. Compton, W. D.; and Arnold, G. W.: Radiation Effects in Fused Silica and α-Al_2O_3. Discussions Faraday Soc. Vol. 31, 1961, p. 130.

17. Zaininger, K. H.; and Holmes-Siedle, A. G.: A Survey of Radiation Effects in Metal-Insulator-Semiconductor Devices. RCA Rev., Vol. 208, June 1967, p. 208.

18. Snow, E. H.; Grove, A. S.; and Fitzgerald, D. J.: Effects of Ionizing Radiation on Oxidized Silicon Surfaces and Planar Devices. Proc. IEEE, Vol. 55, No. 7, July 1967, p. 1168.

19. Speth, A. J.; and Fang, F. F.: Effects of Low-Energy Electron Irradiation on Si-Insulated Gate FETs. Appl. Phys. Letters, Vol. 7, No. 6, Sept. 1965, p. 145.

20. MacDonald, N. C.; and Everhart, T. E.: An Investigation of Electron Beam Irradiation Effects on Metal-Oxide-Semiconductor Transistors. Part I, Electronics Res. Lab., Univ. of California, Berkeley, Calif., Report No. ERL-66-16, 30 Sept. 1966.

21. Wilson, D. K.; Mitchell, J. P.; Cuthbert, J. D.; and Blair, R. R.: Effects of Radiation on Semiconductor Materials and Devices. BTL, AFCRL-67-0068, Dec. 1966.

22. Goodman, A. M.: Photoemission of Holes from Silicon into Silicon Dioxide. Phys. Rev., Vol. 152, No. 2, Dec. 1966, p. 780.

23. Schumacher, B. W.; and Mitra, S. S.: Measuring Thickness and Composition of Thin Surface Films by Means of an Electron Probe. Proc. 1962 Elec. Comp. Conf., Wash., D. C., May 1962, p. 152.

24. Sternglass, E. J.: Backscattering of Kilovolt Electrons from Solids. Phys. Rev., Vol. 95, No. 2, July 1954, p. 345.

25. Williams, R.: Photoemission of Electrons from Silicon into Silicon Dioxide. Phys. Rev., Vol. 140, No. 2A, Oct. 1965, p. A569.

26. Sah, C. T.: Characteristics of the Metal-Oxide-Semiconductor Transistors. IEEE Trans. Elec. Dev., ED-11, July 1964, p. 324.

27. Newman, P. A.; and Wannemacher, H.: Anomalous Radiation Effect in P-Channel MOSFETs under Electron Irradiation. Proc. IEEE, Apr. 1967, p. 562.

28. Dennehy, W. J.; Brucher, G. J.; and Holmes-Siedle, A. G.: A Radiation-Induced Instability in Silicon MOS Transistors, IEEE Trans. Nucl. Sci., NS-13, No. 6, Dec. 1966.

NASA-Langley, 1968 —— 26 CR-1088